SANDIA REPORT
SAND2019-8197
Printed July 2019

Sandia National Laboratories

EMPHASIS™/Nevada Unstructured FEM Implementation Version 2.1.3

C. David Turner, Timothy D. Pointon, Keith L. Cartwright

Prepared by
Sandia National Laboratories
Albuquerque, New Mexico 87185
and Livermore, California 94550

Issued by Sandia National Laboratories, operated for the United States Department of Energy by National Technology & Engineering Solutions of Sandia, LLC.

Available to DOE and DOE contractors from
U.S. Department of Energy
Office of Scientific and Technical Information
P.O. Box 62
Oak Ridge, TN 37831

Telephone: (865) 576-8401
Facsimile: (865) 576-5728
E-Mail: reports@osti.gov
Online ordering: http://www.osti.gov/scitech

Available to the public from
U.S. Department of Commerce
National Technical Information Service
5301 Shawnee Rd
Alexandria, VA 22312

Telephone: (800) 553-6847
Facsimile: (703) 605-6900
E-Mail: orders@ntis.gov
Online order: https://classic.ntis.gov/help/order-methods/

SAND2019-8197
Unlimited Release
Printed July 2019

EMPHASIS™/Nevada Unstructured FEM Implementation Version 2.1.3

Description, Verification, and Validation

C. David Turner, Timothy D. Pointon, Keith L. Cartwright

Electromagnetics and Plasma Physics Analysis

Sandia National Laboratories
P. O. Box 5800
Albuquerque, NM 87185

Abstract

EMPHASIS™/NEVADA is the SIERRA/NEVADA toolkit implementation of portions of the EMPHASIS™ code suite. The purpose of the toolkit implementation is to facilitate coupling to other physics drivers such as radiation transport as well as to better manage code design, implementation, complexity, and important verification and validation processes. This document describes the theory and implementation of the unstructured finite-element method solver, associated algorithms, and selected verification and validation.

Acknowledgement

The author would like to recognize all of the ALEGRA team members for their gracious and willing support through this initial Nevada toolkit-implementation process. Although much of the knowledge needed was gleaned from documentation and code context, they were always willing to consult personally on some of the less obvious issues and enhancements necessary.

Contents

List of Figures

1.0 Introduction

EMPHASIS is a suite of codes for solving Maxwell's equations in a full-field sense, i.e., no approximations. The major codes in the suite include EIGER, QUICKSILVER, and VOLMAX. EIGER is a frequency-domain code and is moving into the SIERRA framework. QUICKSILVER is a rectilinear, structured mesh, Finite-Difference Time-Domain (FDTD) Particle-in-Cell (PIC) code which is moving into the NEVADA framework. VOLMAX is an unstructured, Finite-Element Method (FEM) code (with hybrid FEM/FDTD capability) whose implementation into the NEVADA framework is the subject of this document.

The purposes of moving a code under a framework such as NEVADA are many. At the highest level, these include Configuration Management (CM), Verification & Validation (V&V) tools and processes, and parallelization with domain decomposition. The framework also provides a basic FEM backbone, access to a large, parallel linear system solver such as AZTEC, and basic parsing and I/O. The framework also simplifies the coupling of different types of physics.

The decision as to which framework to follow was not an easy one. Many factors [1] were considered and soon the NEVADA framework emerged as the choice for implementation of the time-domain portion of EMPHASIS. The primary factor was the choice of NEVADA as the Sandia "computational physics" framework. For electromagnetic applications, this includes normal environments (ElectroMagnetic Interference (EMI), ElectroMagnetic Radiation (EMR), ElectroMagnetic Compatibility (EMC)), abnormal environments (lightning), and hostile environments (System-Generated ElectroMagnetic Pulse (SGEMP)) as defined by the Stockpile-to-Target Sequence (STS). SIERRA is the Sandia computational mechanics framework, including the mechanical effects of these environments.

The implementation of the FEM EMPHASIS solver into NEVADA is not simply an effort to port Fortran77-based VOLMAX to C++, nor is it wrapped Fortran77. The code has been completely rewritten in C++ starting from the basic equations and/or algorithms implemented in VOLMAX. The FEM EMPHASIS solver as implemented in NEVADA is referred to as Unstructured Time-Domain ElectroMagnetics (UTDEM).

This document describes the basic electro-magnetic theory, algorithms, and implementation of Release 2.1.0 of UTDEM. It is not meant to be a user manual, although examination of the input files for the Verification section, given in the Appendix, along with the remainder of this document would provide a knowledgeable EM code user with a significant head start toward using the code.

2.0 Fundamental Physics

2.1 Full-field Electromagnetics

The relevant Maxwell equations are

$$\nabla\times\bar{E} = -\mu\frac{\partial}{\partial t}\bar{H} \tag{1}$$

$$\nabla\times\bar{H} = \varepsilon\frac{\partial}{\partial t}\bar{E} + \sigma\bar{E} + \bar{J} \tag{2}$$

$$\nabla\bullet\bar{E} = \frac{\rho}{\varepsilon} \tag{3}$$

$$\nabla\bullet\bar{H} = 0 \tag{4}$$

where $\bar{E}$ is the electric field intensity, $\bar{H}$ is the magnetic field intensity, ρ is the volume charge density, $\bar{J}$ is the volume current, σ is the conductivity, ε is the permittivity of the medium, and μ is the permeability of the medium.

Two basic formulations of the solution of Maxwell's equations have been implemented. These are the unconditionally stable, second-order formulation and the coupled, first-order formulation. The first-order formulation is conditionally stable and must abide by a Courant-type condition for stability.

For the second-order formulation, taking the curl of equation (1) and substitution of equation (2) into the resulting equation yields

$$\nabla\times\left(\frac{1}{\mu_r}\nabla\times\bar{E}\right) = -\mu_0\frac{\partial}{\partial t}\nabla\times H = -\mu_0\frac{\partial}{\partial t}\left(\varepsilon\frac{\partial}{\partial t}\bar{E} + \sigma\bar{E} + \bar{J}\right) \tag{5}$$

Rearranging,

$$\nabla\times\left(\frac{1}{\mu_r}\nabla\times\bar{E}\right) + \frac{\varepsilon_r}{c^2}\frac{\partial^2}{\partial t^2}\bar{E} + \mu_0\sigma\frac{d}{dt}\bar{E} + \mu_0\bar{E}\frac{d\sigma}{dt} = -\mu_0\frac{\partial}{\partial t}\bar{J} \tag{6}$$

where ε_r is the relative permittivity, μ_r is the relative permeability, ε_0 is the permittivity of free space, μ_0 is the permeability of free space, and $c = 1/\sqrt{\mu_0\varepsilon_0}$ is the speed of light.

For the coupled first-order formulation, no second-order equation is formed but instead the two curl equations (1) and (2) are solved coupled in an FDTD leap-frog sense.

3.0 Numerical Solution and Implementation

3.1 FEM Solution for the Second-order Formulation

The FEM formulation of the solution of equation (6) proceeds as follows via the method of weighted residuals and Galerkin's method. The residual is

$$\bar{r} = \nabla\times\left(\frac{1}{\mu_r}\nabla\times\bar{E}\right) + \frac{\varepsilon_r}{c^2}\frac{\partial^2}{\partial t^2}\bar{E} + \mu_0\sigma\frac{d}{dt}\bar{E} + \mu_0\bar{E}\frac{d\sigma}{dt} + \mu_0\frac{\partial}{\partial t}\bar{J} \tag{7}$$

and the weighted residual for the i^{th} weighting function in element e is

$$R^e{}_i = \int_{\Omega e} \overline{W}_i \bullet \bar{r}\, dv =$$

$$\int_{\Omega e}\left(\overline{W}_i \bullet \nabla\times\left(\frac{1}{\mu_r}\nabla\times\bar{E}\right) + \overline{W}_i \bullet \frac{\varepsilon_r}{c^2}\frac{\partial^2}{\partial t^2}\bar{E} + \overline{W}_i \bullet \mu_0\sigma\frac{d}{dt}\bar{E} + \overline{W}_i \bullet \mu_0\bar{E}\frac{d\sigma}{dt} + \overline{W}_i \bullet \mu_0\frac{\partial}{\partial t}\bar{J}\right)dv \tag{8}$$

where $\overline{W}_i$ is the i^{th} weighting function. Invoking Green's first theorem, write

$$\int_{\Omega e} \overline{W}_i \bullet \nabla\times\left(\frac{1}{\mu_r}\nabla\times\bar{E}\right)dv = \int_{\Omega e}\frac{1}{\mu_r}\nabla\times\overline{W}_i \bullet \nabla\times\bar{E}\, dv - \oint_{S_e}\frac{1}{\mu_r}(\overline{W}_i \times \nabla\times\bar{E}) \bullet \hat{n}\, dS \tag{9}$$

so the residual becomes

$$\begin{aligned} R^e{}_i = \int_{\Omega e}\Bigg(&\frac{1}{\mu_r}\nabla\times\overline{W}_i \bullet \nabla\times\bar{E} + \overline{W}_i \bullet \frac{\varepsilon_r}{c^2}\frac{\partial^2}{\partial t^2}\bar{E} + \overline{W}_i \bullet \mu_0\sigma\frac{d}{dt}\bar{E} + \\ &\overline{W}_i \bullet \mu_0\bar{E}\frac{d\sigma}{dt} + \overline{W}_i \bullet \mu_0\frac{\partial}{\partial t}\bar{J}\Bigg)dv - \oint_{S_e}\frac{1}{\mu_r}(\overline{W}_i \times \nabla\times\bar{E}) \bullet \hat{n}\, dS \end{aligned} \tag{10}$$

Using the Sommerfeld radiation condition,

$$\nabla\times\bar{E} + \frac{1}{c}\hat{n}\times\frac{\partial}{\partial t}\bar{E} = 0 \tag{11}$$

the last term in equation (10) becomes

$$-\oint_{S_e}\frac{1}{\mu_r}(\overline{W}_i \times \nabla\times\bar{E}) \bullet \hat{n}\, dS = \oint_{S_e}\frac{1}{c\mu_r}\hat{n}\times\frac{\partial}{\partial t}\bar{E} \bullet \hat{n}\times\overline{W}_i\, dS \tag{12}$$

after application of the vector identity

$$\bar{a} \bullet (\bar{b}\times\bar{c}) = \bar{c} \bullet (\bar{a}\times\bar{b}) \tag{13}$$

The electric field is expanded in the element using the trial functions as follows:

$$\bar{E} = \sum_{i=1}^{m} \overline{W}_j E_j \tag{14}$$

where m is the number of unknowns on the element and $\overline{W}_j$ is the j^{th} trial function and E_j is an unknown coefficient. The trial functions here will turn out to be the edge basis functions and the coefficients the edge field projections.

Applying Galerkin's method by setting the trial and weighting functions equal, substituting for $\bar{E}$ from equation (14), and setting the residual to zero yields the following system

$$\left[\frac{1}{c^2}\int_{\Omega e}\varepsilon_r \bar{W}_i \bullet \bar{W}_j dv\right]\frac{d^2E}{dt^2} + \left[\oint_{S_e}\frac{1}{c\mu_r}\hat{n}\times\bar{W}_i \bullet \hat{n}\times\bar{W}_j dS + \int_{\Omega e}\mu_0\sigma\bar{W}_i \bullet \bar{W}_j dv\right]\frac{\partial E}{\partial t}$$
$$+\left[\int_{\Omega e}\frac{1}{\mu_r}\nabla\times\bar{W}_i \bullet \nabla\times\bar{W}_j dv + \int_{\Omega e}\mu_0\frac{\partial\sigma}{\partial t}\bar{W}_i \bullet \bar{W}_j dv\right]E + \int_{\Omega e}\mu_0\bar{W}_i \bullet \frac{\partial}{\partial t}\bar{J}dv = 0 \quad (15)$$

where E is the coefficient vector and the entire equation has been multiplied through by μ_0. In matrix form after assembly,

$$[T]\frac{d^2E}{dt^2} + [B]\frac{\partial E}{\partial t} + [S]E + F] = 0 \quad (16)$$

The time advance of the above system utilizes a general three-point recurrence scheme for second-order equations [2][3]. This advancement scheme can also be obtained by applying Newmark-Beta approximations for the derivatives in equation (16) as follows:

$$[T]\frac{E_c^{n+1} - 2E_c^n + E_c^{n-1}}{\Delta t^2} + [B]\frac{E_c^{n+1} - E_c^{n-1}}{2\Delta t} + [S]\frac{E_c^{n+1} + 2E_c^n + E_c^{n-1}}{4} + F] = 0 \quad (17)$$

which after some algebra, can be written as

$$E^{n+1} - 2E^n + E^{n-1} +$$
$$4\Delta t\frac{([B] + \Delta t[S])E^n - [B]E^{n-1} + \Delta tF]}{4[T] + 2\Delta t[B] + \Delta t^2[S]} = 0 \quad (18)$$

or,

$$E^{n+1}] - 2E^n] + E^{n-1}] + [M]^{-1}y] = 0 \quad (19)$$

The last term, a sparse, symmetric, positive-definite linear system of equations,

$$[M]x] = y] \quad (20)$$

is solved each time step and equation (19) applied to obtain E^{n+1}. If the constitutive parameters and the mesh are not varying with time, the matrix is filled once and only the right hand side is filled each time step. The filling of the right hand side is facilitated by storing the appropriate matrices multiplying E^n and E^{n+1} in y from equation (18). The new right hand side is then obtained by matrix multiplication. Note that in the implementation,

the matrix [M] and rhs [y] terms in equation (20) have been multiplied through by c^2 for convenience.

Although the second-order formulation is unconditionally stable, practical limitations exist, primarily the fact that the matrix becomes more ill-conditioned as the time step is increased. Solving the system of equation (20) using conjugate-gradient (CG) techniques, therefore, requires increasingly more iterations as the time step increases.

3.2 Full SPICE Circuit Coupling

3.2.1 Implementation: Second-Order Formulation

Implementation of full SPICE-FETD circuit coupling follows that in [4]. The matrices in equation (16) must be partitioned to separate the edge unknowns associated with SPICE loads (subscript *c*) from all other edges (subscript *e*) as follows,

$$\begin{bmatrix} [T_{ee}] & [T_{ec}] \\ [T_{ce}] & [T_{cc}] \end{bmatrix} \frac{d^2}{dt^2} \begin{bmatrix} E_e \\ E_c \end{bmatrix} + \begin{bmatrix} [B_{ee}] & [B_{ec}] \\ [B_{ce}] & [B_{cc}] \end{bmatrix} \frac{\partial}{\partial t} \begin{bmatrix} E_e \\ E_c \end{bmatrix} + \begin{bmatrix} [S_{ee}] & [S_{ec}] \\ [S_{ce}] & [S_{cc}] \end{bmatrix} \begin{bmatrix} E_e \\ E_c \end{bmatrix} + \begin{bmatrix} F_e \\ F_c \end{bmatrix} = 0 \quad (21)$$

After application of the Newmark-Beta time advance, equation (21) can be written as the following two equations where for convenience the vector braces have been left off the *E* terms:

$$[T_{ee}] \frac{E_e^{n+1} - 2E_e^{n} + E_e^{n-1}}{\Delta t^2} + [T_{ec}] \frac{d^2 E_c}{dt^2} + [B_{ee}] \frac{E_e^{n+1} - E_e^{n-1}}{2\Delta t} + [B_{ec}] \frac{dE_c}{dt} + [S_{ee}] \frac{E_e^{n+1} + 2E_e^{n} + E_e^{n-1}}{4} + [S_{ec}] E_c + F_e] = 0 \quad (22)$$

$$[T_{ce}] \frac{E_e^{n+1} - 2E_e^{n} + E_e^{n-1}}{\Delta t^2} + [T_{cc}] \frac{d^2 E_c}{dt^2} + [B_{ce}] \frac{E_e^{n+1} - E_e^{n-1}}{2\Delta t} + [B_{cc}] \frac{dE_c}{dt} + [S_{ce}] \frac{E_e^{n+1} + 2E_e^{n} + E_e^{n-1}}{4} + [S_{cc}] E_c + F_c] = 0 \quad (23)$$

Solving equation (22) for E_e^{n+1} and substitution into equation (23) yields

$$\frac{\left[T_{ce}\right]+\frac{\Delta t}{2}\left[B_{ce}\right]+\frac{\Delta t^2}{4}\left[S_{ce}\right]}{\left[T_{ee}\right]+\frac{\Delta t}{2}\left[B_{ee}\right]+\frac{\Delta t^2}{4}\left[S_{ee}\right]}\Big\{-\left[T_{ee}\right](-2E_e^{\,n}+E_e^{\,n-1})-\Delta t^2\left[T_{ec}\right]\frac{d^2E_c}{dt^2}+$$

$$\frac{\Delta t}{2}\left[B_{ee}\right]E_e^{\,n-1}-\Delta t^2\left[B_{ec}\right]\frac{dE_c}{dt}-\frac{\Delta t^2}{4}\left[S_{ee}\right](2E_e^{\,n}+E_e^{\,n-1})-\Delta t^2\left[S_{ec}\right]E_c-\Delta t^2\ F_e]\Big\} \tag{24}$$

$$=-\left[T_{ce}\right](-2E_e^{\,n}+E_e^{\,n-1})-\Delta t^2\left[T_{cc}\right]\frac{d^2E_c}{dt^2}+\frac{\Delta t}{2}\left[B_{ce}\right]E_e^{\,n-1}-\Delta t^2\left[B_{cc}\right]\frac{dE_c}{dt}-$$

$$\frac{\Delta t^2}{4}\left[S_{ce}\right](2E_e^{\,n}+E_e^{\,n-1})-\Delta t^2\left[S_{cc}\right]\ E_c\ -\Delta t^2\ F_c]$$

Collecting terms and letting

$$\left[\left[T_{ce}\right]+\frac{\Delta t}{2}\left[B_{ce}\right]+\frac{\Delta t^2}{4}\left[S_{ce}\right]\right]\ =\ \left[M_{ce}\right] \tag{25}$$

$$\left[\left[T_{ee}\right]+\frac{\Delta t}{2}\left[B_{ee}\right]+\frac{\Delta t^2}{4}\left[S_{ee}\right]\right]^{-1}\ =\ \left[M_{ee}\right]^{-1} \tag{26}$$

$$\left[M_{ee}\right]^{-1}\left[T_{ec}\right]\ =\ \left[M_{Tec}\right] \tag{27}$$

$$\left[M_{ee}\right]^{-1}\left[B_{ec}\right]\ =\ \left[M_{Bec}\right] \tag{28}$$

$$\left[M_{ee}\right]^{-1}\left[S_{ec}\right]\ =\ \left[M_{Sec}\right] \tag{29}$$

equation (24) becomes

$$\Big\{-\left[M_{ce}\right]\left[M_{Tec}\right]+\left[T_{cc}\right]\Big\}\frac{d^2E_c}{dt^2}+\Big\{-\left[M_{ce}\right]\left[M_{Bec}\right]+\left[B_{cc}\right]\Big\}\frac{dE_c}{dt}+\ F_c]\ =$$

$$\left[M_{ce}\right]\left[M_{ee}\right]^{-1}\Big\{\frac{1}{\Delta t^2}\left[T_{ee}\right](-2E_e^{\,n}+E_e^{\,n-1})-\frac{1}{2\Delta t}\left[B_{ee}\right]E_e^{\,n-1}+$$

$$\frac{1}{4}\left[S_{ee}\right](2E_e^{\,n}+E_e^{\,n-1})+\ F_e]\Big\}-\Big\{-\left[M_{ce}\right]\left[M_{Sec}\right]+\left[S_{cc}\right]\Big\}E_c- \tag{30}$$

$$\frac{1}{\Delta t^2}\left[T_{ce}\right](-2E_e^{\,n}+E_e^{\,n-1})+\frac{1}{2\Delta t}\left[B_{ce}\right]E_e^{\,n-1}-$$

$$\frac{1}{4}\left[S_{ce}\right](2E_e^{\,n}+E_e^{\,n-1})$$

where, from equations (15) and (16),

$$F_c = \int_{\Omega e} \overline{W}_i \bullet \frac{\partial}{\partial t} \bar{J} dv \tag{31}$$

Here, the matrix terms in equation (30) and (31) have not been multiplied by μ_0 as they were for equations (15) and (18). Extracting the lumped-edge load current from the integral in equation (31),

$$F_c = \int_{\Omega e} \overline{W}_i \bullet \frac{\partial}{\partial t} \bar{J} dv + \frac{dI_c}{dt} \tag{32}$$

where I_c is the lumped-element edge current. Note that the first bracketed term on the right hand side of equation (30) is proportional to the solution of the non-SPICE edges without consideration of the SPICE edges, $\tilde{E}_e^{n+1}$:

$$\begin{aligned} &\{-[M_{ce}][M_{Tec}]+[T_{cc}]\}\frac{d^2E_c}{dt^2}+\{-[M_{ce}][M_{Bec}]+[B_{cc}]\}\frac{dE_c}{dt}+F_c]= \\ &[M_{ce}]\tilde{E}_e^{n+1}-\{-[M_{ce}][M_{Sec}]+[S_{cc}]\}E_c- \\ &\frac{1}{\Delta t^2}[T_{ce}](-2E_e^n+E_e^{n-1})+\frac{1}{2\Delta t}[B_{ce}]E_e^{n-1}-\frac{1}{4}[S_{ce}](2E_e^n+E_e^{n-1}) \end{aligned} \tag{33}$$

Equation (33) has the form

$$\left[C_d\right]\frac{d^2E_c}{dt^2} + \left[G_d\right]\frac{dE_c}{dt} + F_c] = F] - \left[L_d\right]^{-1}E_c \tag{34}$$

which can now be written as

$$\left[C_d\right]\frac{d^2E_c}{dt^2} + \left[G_d\right]\frac{dE_c}{dt} + \frac{dI_c}{dt} = F] - \int_{\Omega e} \overline{W}_i \bullet \frac{\partial}{\partial t} \bar{J} dv - \left[L_d\right]^{-1}E_c = F'] - \left[L_d\right]^{-1}E_c \tag{35}$$

Defining

$$\frac{dI_d}{dt} = F' - \left[L_d\right]^{-1}E_c \tag{36}$$

then

$$I_d = \left[C_d\right]\frac{dE_c}{dt} + \left[G_d\right]E_c + I_c \tag{37}$$

$$F' = [M_{ce}]\ddot{E}_e^{n+1} - \frac{1}{\Delta t^2}[T_{ce}](-2E_e^n + E_e^{n-1}) + \frac{1}{2\Delta t}[B_{ce}]E_e^{n-1} - \frac{1}{4}[S_{ce}](2E_e^n + E_e^{n-1}) \tag{38}$$

In the time advance of equations (36) and (37), the equations are assumed centered at time *n* and Newmark-Beta approximations are used. For equation (36),

$$I_d^{n+1} = I_d^{n-1} + 2\Delta t\left(F' - [L_d]^{-1}\left(\frac{E_c^{n+1} + 2E_c^n + E_c^{n-1}}{4}\right)\right) \tag{39}$$

In equation (37), which will be solved using SPICE, the Newmark-Beta approximation is used for $I^n{}_d$,

$$I_d^n = \frac{I_d^{n+1} + 2I_d^n + I_d^{n-1}}{4} = \frac{1}{4}\left(2I_d^n + 2I_d^{n-1} + 2\Delta t\left(F' - [L_d]^{-1}E_c\right)\right) \tag{40}$$

after substitution from equation (39) but returning to the continuous form for E_c. Equation (37) (still centered at n) now becomes

$$I'^n_d = \frac{1}{4}\left(2I_d^n + 2I^{n-1}_d + 2\Delta t F'\right) = [C_d]\frac{dE_c}{dt} + [G_d]E_c + I_c + \frac{\Delta t}{2}[L_d]^{-1}E_c \tag{41}$$

An equivalent circuit representing equation (41) for a single SPICE-loaded edge is shown in Figure 1 . The $[L_d]^{-1}\,E_c$ term is treated as a voltage-dependent current source. In general, the matrices $[C_d]$, $[G_d]$, and $[L_d]^{-1}$ are not symmetric. Consequently, additional dependent sources are necessary in the equivalent circuit if more than one SPICE load exists. An example for two SPICE loads is shown in Figure 2 , shown without the $[L_d]^{-1}\,E_c$ term sources for simplicity.

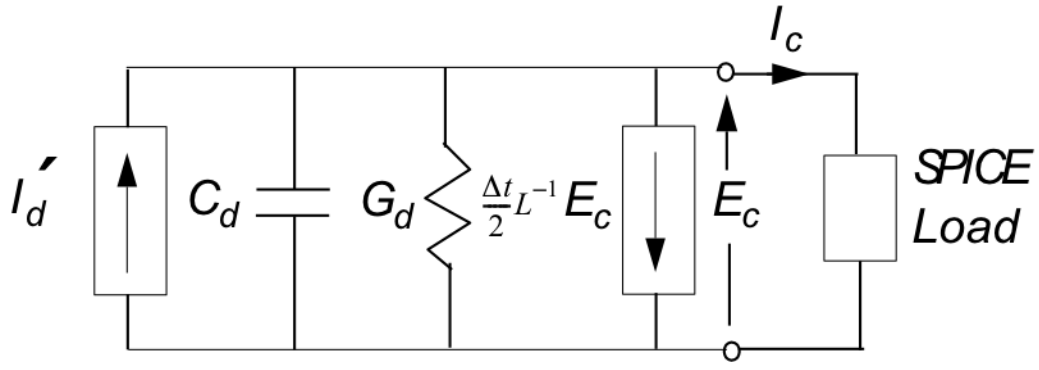

Figure 1 . Equivalent circuit for FETD-SPICE interface with single load.

$$\begin{bmatrix} I_{d1} \\ I_{d2} \end{bmatrix} = \begin{bmatrix} C_{11} & C_{12} \\ C_{21} & C_{22} \end{bmatrix} \begin{bmatrix} \dot{E}_{c1} \\ \dot{E}_{c2} \end{bmatrix} + \begin{bmatrix} G_{11} & G_{12} \\ G_{21} & G_{22} \end{bmatrix} \begin{bmatrix} E_{c1} \\ E_{c2} \end{bmatrix} + \begin{bmatrix} I_{c1} \\ I_{c2} \end{bmatrix}$$

$$I_{d1} = C_{11}\dot{E}_{c1} + \frac{C_{12}}{C_{22}} I_{c22} + G_{11}E_{c1} + \frac{G_{12}}{G_{22}} I_{g22} + I_{c1}$$

$$I_{d2} = C_{22}\dot{E}_{c2} + \frac{C_{21}}{C_{11}} I_{c11} + G_{22}E_{c2} + \frac{G_{21}}{G_{11}} I_{g11} + I_{c2}$$

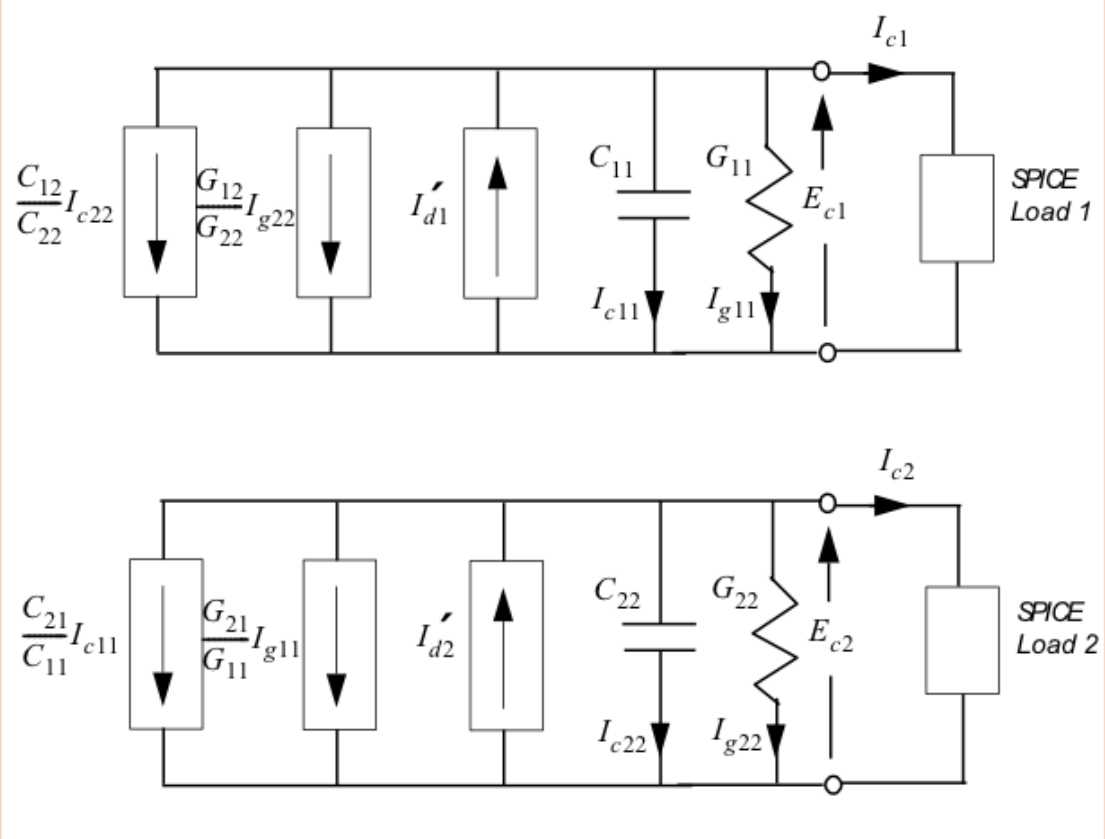

Figure 2 . Equivalent circuit for FETD-SPICE interface with two loads.

The solution approach for each time cycle is as follows. First, $\tilde{E}_e^{\,n+1}$ is advanced as if no SPICE edges exist. Using previous values of E_e^{n-1}, E_e^n, and the now advanced $\tilde{E}_e^{\,n+1}$, F' is computed. Then, with I_d^n, and I_d^{n-1}, equation (41) is solved using SPICE and the drive circuit as in Figure 1 returning the advanced SPICE-edge voltage E_c^{n+1}. Now, I_d^{n+1} is advanced using equation (39). The final step is to correct the non-SPICE edges for the

existance of the SPICE-edges. This is accomplished using equation (22) and the just advanced E_c^{n+1} along with previous values E_c^n and E_c^{n-1} to solve just the E_c terms and add them to the $\tilde{E}_e^{n+1}$ solution vector.

Note that when the E_c results are used in equation (22), a solve is required. This solve can be accomplished using the previously computed $[M_{Tec}]$, $[M_{Bec}]$, and $[M_{Sec}]$ matrices as follows:

$$E_e^{n+1} = \tilde{E}_e^{n+1} + \left[M_{Tec}\right]\frac{d^2E_c}{dt^2} + \left[M_{Bec}\right]\frac{dE_c}{dt} + \left[M_{Sec}\right]E_c \tag{42}$$

The Newmark-Beta approximations for the derivatives of E_c are used in equation (42),

$$\frac{d^2E_c}{dt^2} = \frac{E_c^{n+1} - 2E_c^{n} + E_c^{n-1}}{\Delta t^2} \tag{43}$$

$$\frac{dE_c}{dt} = \frac{E_c^{n+1} - E_c^{n-1}}{2\Delta t} \tag{44}$$

$$E_c = \frac{E_c^{n+1} + 2E_c^{n} + E_c^{n-1}}{4} \tag{45}$$

These correction terms can be thought of as a part of F in equation (18). Consequently, they must be scaled by $4\Delta t^2$ to agree with the scaling in the original system.

Referring to equations (25)-(29), if there are n normal edges and m spice-loaded edges, then $[M_{ce}]$ is $m \times n$, $[T_{ec}]$, $[B_{ec}]$, and $[S_{ec}]$ are $n \times m$ while $[M_{ee}]^{-1}$ is $n \times n$, making $[M_{Tec}]$, $[M_{Bec}]$, and $[M_{Sec}]$ all $n \times m$ matrices. If there is a single SPICE-loaded edge in the space, then the $[M]$'s are $n \times 1$ vectors and equation (30) is a scalar equation for a single unknown E_c.

The above implementation has been shown to be unconditionally stable for a single SPICE-loaded edge. However, multiple SPICE-loaded edges exhibit a slow instability the source of which has not been identified. Therefore, the code is presently limited to a single SPICE-loaded edge.

3.2.2 Implementation: First-Order Formulation

The SPICE-FETD interface has not yet been implemented for the first-order formulation.

3.3 Artuzi Late-time Stability Formulation

It is well known that the wave equation (6) is subject to linearly increasing spurious solutions [5]. This "instability" is normally only noticed for simulations lasting a very long time with a large number of time cycles. It can often be controlled using a very small solution tolerance for the conjugate-gradient solve in equation (20). However, when attempting to utilize the inherent unconditional stability of the second-order formulation to reach the quasi-static or very low-frequency regime the issue can often been seen and not easily controlled.

3.3.1 Implementation: Second-Order Formulation

Artuzi [5] reformulates the wave equation in terms of the integral of E such that the resulting equation does not support the spurious solution. Following [5], the formulation differs from the previously described second-order formulation in that rather than storing the vectors E^{n+1}, E^{n}, and E^{n-1} the relevant vectors are u^{n}, $E^{n+1/2}$, and w^{n+1}. Equation (16) becomes

$$\left[T\right]\frac{d^2 w}{dt^2} + [B]\frac{\partial w}{\partial t} + [S]w + F] = 0 \tag{46}$$

$$w = \int_{-\infty}^{t} E dt \tag{47}$$

Therefore,

$$E = \frac{\partial w}{\partial t} \qquad u = \frac{\partial E}{\partial t} = \frac{\partial^2 w}{\partial t^2} \tag{48}$$

Manipulating equation (46) using Newmark approximations and

$$u^{n} = \frac{E^{n+1/2} - E^{n-1/2}}{\Delta t}, \quad E^{n+1/2} = \frac{w^{n+1} - w^{n}}{\Delta t}, \text{ so } u^{n} = \frac{w^{n+1} - 2w^{n} + w^{n-1}}{\Delta t^2},$$

$$\left[T\right]\frac{w^{n+1} - 2w^{n} + w^{n-1}}{\Delta t^2} + [B]\frac{w^{n+1} - w^{n-1}}{2\Delta t} + [S]\frac{w^{n+1} + 2w^{n} + w^{n-1}}{4} + F] = 0 \tag{49}$$

$$\left[T\right]u^n + \frac{[B]\Delta t}{2}\frac{w^{n+1} - w^{n-1}}{\Delta t^2} - \frac{[B]\Delta t}{2}\frac{2w^n}{\Delta t^2} + \frac{[B]\Delta t}{2}\frac{2w^n}{\Delta t^2} + \frac{[B]\Delta t}{2}\frac{2w^{n-1}}{\Delta t^2} - \frac{[B]\Delta t}{2}\frac{2w^{n-1}}{\Delta t^2} + [S]\frac{w^{n+1} + 2w^n + w^{n-1}}{4} + F] = 0 \tag{50}$$

$$\left[T\right]u^n + \frac{[B]\Delta t}{2}\frac{w^{n+1} - 2w^n + w^{n-1}}{\Delta t^2} + [B]\frac{w^n}{\Delta t} - [B]\frac{w^{n-1}}{\Delta t} + [S]\frac{w^{n+1} + 2w^n + w^{n-1}}{4} + F] = 0 \tag{51}$$

$$\left[T\right]u^n + \frac{[B]\Delta t}{2}u^n + [B]\frac{w^n}{\Delta t} - [B]\frac{w^{n-1}}{\Delta t} + \frac{[S]\Delta t^2}{4}\frac{w^{n+1} + 2w^n + w^{n-1}}{\Delta t^2} - \frac{[S]\Delta t^2}{4}\frac{2w^n}{\Delta t^2} + \frac{[S]\Delta t^2}{4}\frac{2w^n}{\Delta t^2} + F] = 0 \tag{52}$$

$$\left[T\right]u^n + \frac{[B]\Delta t}{2}u^n + [B]\frac{w^n}{\Delta t} - [B]\frac{w^{n-1}}{\Delta t} + \frac{[S]\Delta t^2}{4}\frac{w^{n+1} - 2w^n + w^{n-1}}{\Delta t^2} + \frac{[S]\Delta t^2}{4}\frac{2w^n}{\Delta t^2} + \frac{[S]\Delta t^2}{4}\frac{2w^n}{\Delta t^2} + F] = 0 \tag{53}$$

$$\left[T\right]u^n + \frac{[B]\Delta t}{2}u^n + \frac{[S]\Delta t^2}{4}u^n + [B]\frac{w^n}{\Delta t} - [B]\frac{w^{n-1}}{\Delta t} + [S]w^n + F] = 0 \tag{54}$$

$$\left[T\right]u^n + \frac{[B]\Delta t}{2}u^n + \frac{[S]\Delta t^2}{4}u^n + [B]E^{n-1/2} + [S]w^n + F] = 0 \tag{55}$$

Now, the system becomes

$$(4T + 2\Delta tB + \Delta t^2 S)u^n = -4F_n - 4BE^{n-1/2} - 4Sw^n \tag{56}$$

So the system matrix looks exactly as it did before in equation (18), only the rhs changes while now solving for u^n directly. Once obtained, it is used to update the others as

$$E^{n+1/2} = E^{n-1/2} + \Delta t u^n \qquad w^{n+1} = w^n + \Delta t E^{n+1/2} \tag{57}$$

Scaling factors change slightly from before and note that the edge projections (E's) are now one-half cycle advanced. Most boundary conditions and sources are affected as well.

Even though this scheme can improve the late-time stability performance, it often does not completely eliminate it. Keying off a statement by Artuzi [5] that the spurious solution is isolated in the Artuzi variable w, eliminating the term $4Sw^n$ from equation (56) has some interesting implications. Equation (56) without losses for simplicity is

$$\left(T + \frac{\Delta t^2}{4} S\right) u^n = -F_n \tag{58}$$

after eliminating the $4Sw^n$ term. This corresponds to a continuous equation of the form

$$-\frac{\Delta t^2}{4} \nabla \times \left(\frac{1}{\mu} \nabla \times \frac{\partial E}{\partial t}\right) = \varepsilon \frac{\partial E}{\partial t} + J \tag{59}$$

To have a valid Ampere's law, this implies that in this scheme "H" is now

$$H_{ELF} = -\frac{\Delta t^2}{4\mu} \nabla \times \frac{\partial E}{\partial t} \tag{60}$$

So, a new "low-frequency" H is now defined by a derivative of the curl of E rather than an integral. As odd as this seems, it is mathematically sound and indeed does produce the correct magnetic fields in the low-frequency limit. It is important to remember that this only applies for low frequencies, where the wavelength is much, much, much larger than the objects of interest.

3.3.2 Implementation: First-Order Formulation

The Artuzi correction has not been implemented for the first-order formulation.

3.4 FEM Solution for the First-Order Formulation

In the expansion for the electric field in equation (14), the $\overline{W}_j$ represent edge basis functions and m is the number of edges on the element. For the first-order formulation, a similar expansion for magnetic field is developed using face basis functions,

$$\overline{H} = \sum_{j=1}^{n} \overline{W}_j^f H_j \tag{61}$$

where n is the number of faces on the element, the $\overline{W}_j^f$ represent the face basis functions, and H_j is the magnetic field scalar projection through the element face. Following [6], letting $e]$ represent the vector of unknown edge projections on elements and $b]$ represent the vector of unknown face projections, a discrete analog of equation (1) can be written,

$$[C]e] = \frac{\partial}{\partial t} b] \tag{62}$$

where $[C]$ is a sparse matrix in which the non-zero elements are only ± 1 . $[C]$ has number-of-faces rows and number-of-edges columns and represents the circulation of electric-field edge projections about magnetic-field face projections, i.e., Faraday's law.

For the other Maxwell curl equation (2), Ampere's law, a classic weak form can be derived like the following:

$${}^t[C][\mu]^{-1} b] = \frac{\partial}{\partial t}[\varepsilon]e] + [\sigma]e] + \bar{J} \tag{63}$$

where ${}^t[C]$ is the transpose of $[C]$, $[\mu]^{-1}$, and $[\varepsilon]$ are the "mass" matrices

$$[\varepsilon] = \int_{\Omega e} \varepsilon \overline{W}_i \bullet \overline{W}_j dv \tag{64}$$

$$[\mu]^{-1} = \int_{\Omega e} \frac{1}{\mu} \overline{W}_i^f \bullet \overline{W}_j^f dv \tag{65}$$

and $[\sigma]$ is the matrix

$$[\sigma] = \int_{\Omega e} \sigma \overline{W}_i \bullet \overline{W}_j dv \tag{66}$$

Equations (62) and (63) lead to the following advancement equations:

$$b]_{n+\frac{1}{2}} = b]_{n-\frac{1}{2}} - \Delta t[C]e]_n \tag{67}$$

$$e]_{n+1} = (2[\varepsilon] + \Delta t[\sigma])^{-1} \left[(2[\varepsilon] - \Delta t[\sigma])\bar{e}_n + 2\Delta t\left({}^t[C][\mu]^{-1} b]_{n+\frac{1}{2}} - \bar{J}_{n+\frac{1}{2}} \right) \right] \tag{68}$$

where the inverse of $(2[\varepsilon] + \Delta t[\sigma])$ is required and can be obtained using techniques suitable for sparse, symmetric, positive-definite matrices such as CG.

As noted previously, the first-order formulation is conditionally stable and must abide by the Courant condition.

3.5 Vector Finite Elements

3.5.1 Edge-based Vector Basis Functions for Tetrahedra

To evaluate the elemental integrals in equations (15) and (64)-(66), the arbitrary tetrahedral element is transformed to the corresponding master element as shown in Figure 3 . This transformation is performed through the Jacobian of the transformation. All integrals are performed numerically using Gauss-quadrature integration over the master element. The assumed edge and face orientations are shown in Figure 3 for edges E1-E6 and faces F1-F4.

The Lagrangian interpolation functions for a general, linear element are

$$L_j(x, y, z) = \frac{1}{6V}(a_j + b_j x + c_j y + d_j z) \tag{69}$$

for j=1, 2, 3, 4, where the coefficients a_j, b_j, c_j, and d_j are determined by assuming a nodal-based scheme and generating four equations based on the unknown value at each node. V is the element volume.

For the master tetrahedral element, the interpolation functions simplify to

$$G_1(\xi, \eta, \zeta) = 1 - \xi - \eta - \zeta \tag{70}$$

$$G_2(\xi, \eta, \zeta) = \xi \tag{71}$$

$$G_3(\xi, \eta, \zeta) = \eta \tag{72}$$

$$G_4(\xi, \eta, \zeta) = \zeta \tag{73}$$

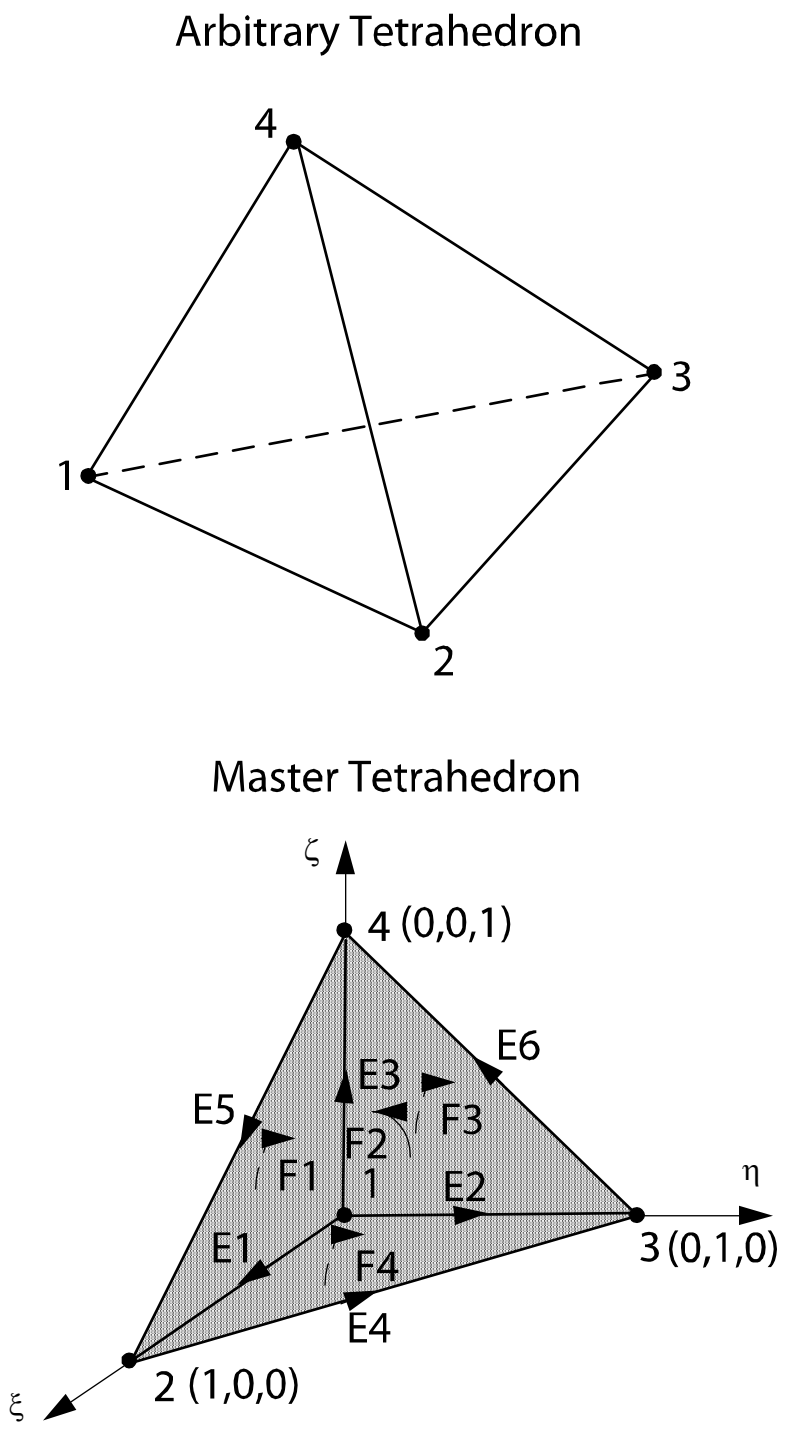

Figure 3 . Vector tetrahedral element.

The global to local coordinate transformation between the arbitrary and the master tetrahedron is given by

$$x = \sum_{i=1}^{4} x_i G_i(\xi, \eta, \zeta) \tag{74}$$

$$y = \sum_{i=1}^{4} y_i G_i(\xi, \eta, \zeta) \tag{75}$$

$$z = \sum_{i=1}^{4} z_i G_i(\xi, \eta, \zeta) \tag{76}$$

Here, nodes 1, 2, 3, and 4 correspond to the corners of the tetrahedron as appropriate for a linear tetrahedron. Using the chain rule of partial differentiation

$$\frac{\partial G_i}{\partial \xi} = \frac{\partial G_i}{\partial x}\frac{\partial x}{\partial \xi} + \frac{\partial G_i}{\partial y}\frac{\partial y}{\partial \xi} + \frac{\partial G_i}{\partial z}\frac{\partial z}{\partial \xi} \tag{77}$$

$$\frac{\partial G_i}{\partial \eta} = \frac{\partial G_i}{\partial x}\frac{\partial x}{\partial \eta} + \frac{\partial G_i}{\partial y}\frac{\partial y}{\partial \eta} + \frac{\partial G_i}{\partial z}\frac{\partial z}{\partial \eta} \tag{78}$$

$$\frac{\partial G_i}{\partial \zeta} = \frac{\partial G_i}{\partial x}\frac{\partial x}{\partial \zeta} + \frac{\partial G_i}{\partial y}\frac{\partial y}{\partial \zeta} + \frac{\partial G_i}{\partial z}\frac{\partial z}{\partial \zeta} \tag{79}$$

or,

$$\begin{bmatrix} \frac{\partial G_i}{\partial \xi} \\ \frac{\partial G_i}{\partial \eta} \\ \frac{\partial G_i}{\partial \zeta} \end{bmatrix} = \begin{bmatrix} \frac{\partial x}{\partial \xi} & \frac{\partial y}{\partial \xi} & \frac{\partial z}{\partial \xi} \\ \frac{\partial x}{\partial \eta} & \frac{\partial y}{\partial \eta} & \frac{\partial z}{\partial \eta} \\ \frac{\partial x}{\partial \zeta} & \frac{\partial y}{\partial \zeta} & \frac{\partial z}{\partial \zeta} \end{bmatrix} \begin{bmatrix} \frac{\partial G_i}{\partial x} \\ \frac{\partial G_i}{\partial y} \\ \frac{\partial G_i}{\partial z} \end{bmatrix} = [\boldsymbol{J}] \begin{bmatrix} \frac{\partial G_i}{\partial x} \\ \frac{\partial G_i}{\partial y} \\ \frac{\partial G_i}{\partial z} \end{bmatrix} \Rightarrow \tilde{\nabla} G_i = [\boldsymbol{J}] \nabla G_i \tag{80}$$

which relates the gradient of G between global and local coordinates through the Jacobian matrix [*J*]. Here, $\tilde{\nabla} G_i$ is the gradient of G in the local (master) coordinates and ∇G_i is the gradient of G in the global (arbitrary) coordinates.

[*J*] can be evaluated by taking the partial derivatives of equations (74)-(76) as

$$[\boldsymbol{J}] = \begin{bmatrix} \frac{\partial}{\partial \xi}\sum_{i=1}^{4} G_i(\xi,\eta,\zeta)x_i & \frac{\partial}{\partial \xi}\sum_{i=1}^{4} G_i(\xi,\eta,\zeta)y_i & \frac{\partial}{\partial \xi}\sum_{i=1}^{4} G_i(\xi,\eta,\zeta)z_i \\ \frac{\partial}{\partial \eta}\sum_{i=1}^{4} G_i(\xi,\eta,\zeta)x_i & \frac{\partial}{\partial \eta}\sum_{i=1}^{4} G_i(\xi,\eta,\zeta)y_i & \frac{\partial}{\partial \eta}\sum_{i=1}^{4} G_i(\xi,\eta,\zeta)z_i \\ \frac{\partial}{\partial \zeta}\sum_{i=1}^{4} G_i(\xi,\eta,\zeta)x_i & \frac{\partial}{\partial \zeta}\sum_{i=1}^{4} G_i(\xi,\eta,\zeta)y_i & \frac{\partial}{\partial \eta}\sum_{i=1}^{4} G_i(\xi,\eta,\zeta)z_i \end{bmatrix} \tag{81}$$

$$= \begin{bmatrix} \frac{\partial G_1}{\partial \xi} & \frac{\partial G_2}{\partial \xi} & \frac{\partial G_3}{\partial \xi} & \frac{\partial G_4}{\partial \xi} \\ \frac{\partial G_1}{\partial \eta} & \frac{\partial G_2}{\partial \eta} & \frac{\partial G_3}{\partial \eta} & \frac{\partial G_4}{\partial \eta} \\ \frac{\partial G_1}{\partial \zeta} & \frac{\partial G_2}{\partial \zeta} & \frac{\partial G_3}{\partial \zeta} & \frac{\partial G_4}{\partial \zeta} \end{bmatrix} \begin{bmatrix} x_1 & y_1 & z_1 \\ x_2 & y_2 & z_2 \\ x_3 & y_3 & z_3 \\ x_4 & y_4 & z_4 \end{bmatrix} = \begin{bmatrix} -1 & 1 & 0 & 0 \\ -1 & 0 & 1 & 0 \\ -1 & 0 & 0 & 1 \end{bmatrix} \begin{bmatrix} x_1 & y_1 & z_1 \\ x_2 & y_2 & z_2 \\ x_3 & y_3 & z_3 \\ x_4 & y_4 & z_4 \end{bmatrix} = \begin{bmatrix} x_2 - x_1 & y_2 - y_1 & z_2 - z_1 \\ x_3 - x_1 & y_3 - y_1 & z_3 - z_1 \\ x_4 - x_1 & y_4 - y_1 & z_4 - z_1 \end{bmatrix}$$

The 6V term in equation (69) is given by

$$\begin{aligned} 6V = det([\boldsymbol{J}]) = \\ (x_2 - x_1)[(y_3 - y_1)(z_4 - z_1) - (y_4 - y_1)(z_3 - z_1)] + \\ (x_3 - x_1)[(y_4 - y_1)(z_2 - z_1) - (y_2 - y_1)(z_4 - z_1)] + \\ (x_4 - x_1)[(y_2 - y_1)(z_3 - z_1) - (y_3 - y_1)(z_2 - z_1)] \end{aligned} \tag{82}$$

and the inverse transformation for the gradient is given by

$$\begin{bmatrix} \frac{\partial G_i}{\partial x} \\ \frac{\partial G_i}{\partial y} \\ \frac{\partial G_i}{\partial z} \end{bmatrix} = [\boldsymbol{J}]^{-1} \begin{bmatrix} \frac{\partial G_i}{\partial \xi} \\ \frac{\partial G_i}{\partial \eta} \\ \frac{\partial G_i}{\partial \zeta} \end{bmatrix} \Rightarrow \nabla G_i = [\boldsymbol{J}]^{-1} \tilde{\nabla} G_i \tag{83}$$

For the edge-based vector master tetrahedron, the expansion or basis functions are derived from the Lagrangian interpolation functions as follows [6][7]:

$$\bar{N}_i = G_{i1}\nabla G_{i2} - G_{i2}\nabla G_{i1} \tag{84}$$

for i = 1-6, where i is the edge number and $i1$ and $i2$ are the nodes associated with the i^{th} edge.

Using some vector calculus, the curls of the edge basis functions are given by

$$\nabla\times\bar{N}_i = 2\nabla G_{i1} \times \nabla G_{i2} \tag{85}$$

These basis functions are used to expand the electric field within an element as in equation (14) with the $\bar{W}_j$ replaced by $\bar{N}_j$. The unique features which make this type of basis function ideal for electromagnetics simulation are 1) the fact that $\bar{N}_j$ has a tangential component only along the j^{th} edge and none along all the other element edges, thus guaranteeing the continuity of tangential electric field across all element edges, and 2) each $\bar{N}_j$ is divergence free, satisfying $\nabla\cdot\bar{N}_j = 0$ within the element.

3.5.2 Hierarchical Vector Basis Functions for Tetrahedra

The edge basis functions in equation (84) are referred to as Whitney elements with a single degree of freedom per edge. Alternatively, they are described as 0th order or 1st order mixed in that they are constant along an edge and linear across the element. This results in more constant than linear behavior and consequently only a linear spatial convergence rate. Addition of six additional basis functions in a hierarchical sense brings the element to full 1st order and the solution to quadratic or 2nd order spatial convergence. However, this adds an additional degree of freedom on each edge and consequently doubles the number of unknowns in the system.

The next six hierarchical basis functions are defined by [8]

$$\bar{N}_i = G_{i1}\nabla G_{i2} + G_{i2}\nabla G_{i1}$$

for i = 1-6, where i is the edge number and $i1$ and $i2$ are the nodes associated with the i^{th} edge. The curls of these six basis functions are identically zero.

3.5.3 Face-based Vector Basis Functions for Tetrahedra

For the first-order formulation, the face-based tetrahedral basis functions are required. They are given by [6]

$$\bar{N}^f_i = 2(G_{i1}(\nabla G_{i2} \times \nabla G_{i3}) + G_{i2}(\nabla G_{i3} \times \nabla G_{i1}) + G_{i3}(\nabla G_{i1} \times \nabla G_{i2})) \tag{86}$$

where i is the face number and $i1$, $i2$, and $i3$ are nodes associated with the i'th face.

3.5.4 Edge-based Vector Basis Functions for Pyramids

Similar to the tetrahedron, the arbitrary pyramid is transformed to the master pyramid as shown in Figure 4 . The assumed edge and face orientations are also shown in Figure 4 for edges E1-E8 and faces F1-F5.

Also like the tetrahedron, the vector basis functions for the pyramid are derived from the nodal expansion functions [9][10]. Using the following transformation,

$$u3 = 1 - \zeta \tag{87}$$

$$u2 = y(1 - u3) \tag{88}$$

$$u1 = x(1 - u3) \tag{89}$$

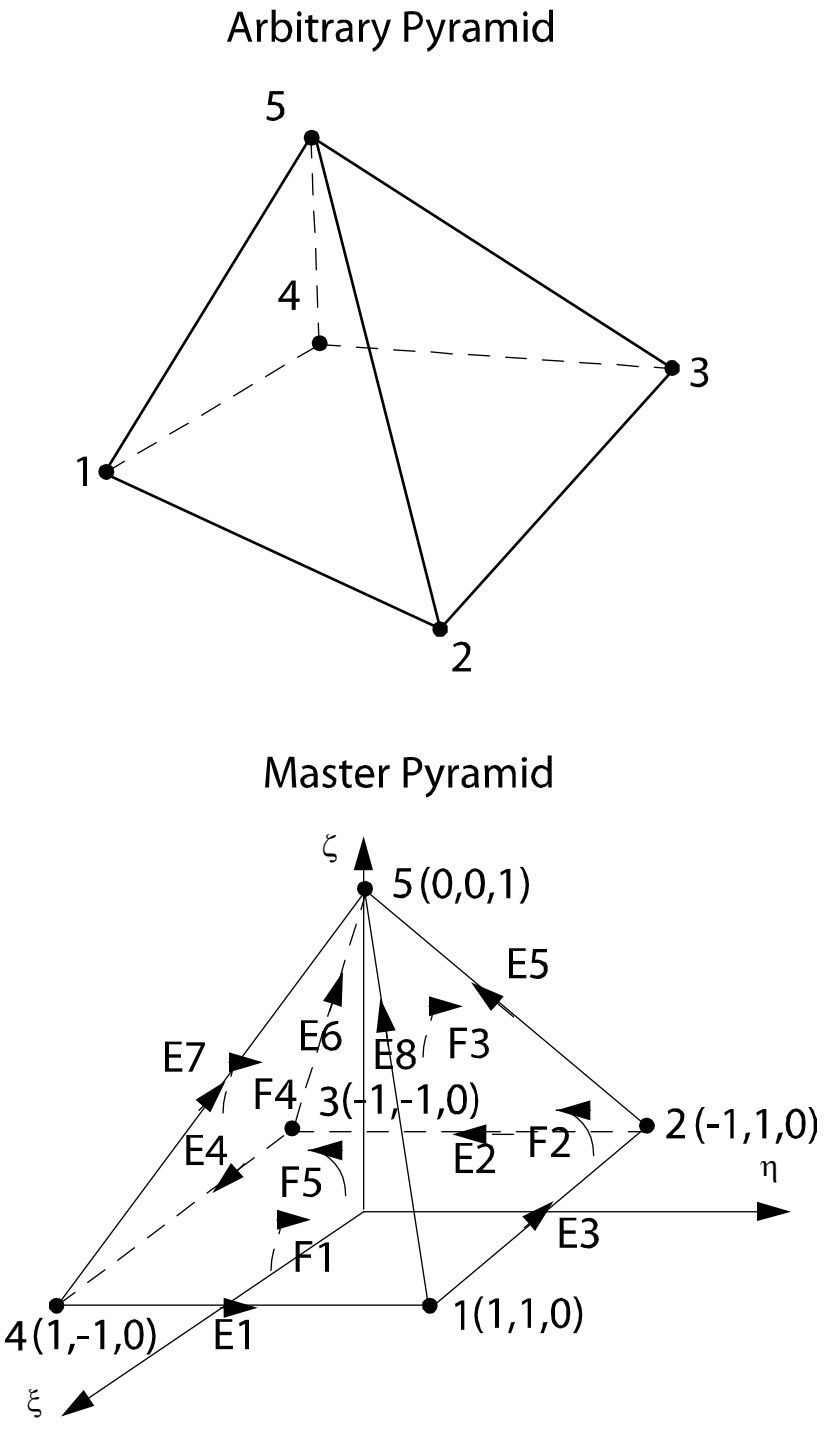

Figure 4 . Vector pyramidal element.

the nodel-based interpolation functions for the pyramid are

$$G_1(\xi, \eta, \zeta) = u1 \tag{90}$$

$$G_2(\xi, \eta, \zeta) = u2 \tag{91}$$

$$G_3(\xi, \eta, \zeta) = 1 - u1 - u3 \tag{92}$$

$$G_4(\xi, \eta, \zeta) = 1 - u2 - u3 \tag{93}$$

$$G_5(\xi, \eta, \zeta) = u3 \tag{94}$$

From these, the following edge-based vector basis functions for the master pyramid are derived:

$$\bar{N}_1 = \frac{G_4 G_1 \nabla G_2 - G_1 G_2 \nabla G_4}{1 - G_5} \tag{95}$$

$$\bar{N}_2 = \frac{G_2 G_3 \nabla G_4 - G_3 G_4 \nabla G_2}{1 - G_5} \tag{96}$$

$$\bar{N}_3 = \frac{G_1 G_2 \nabla G_3 - G_2 G_3 \nabla G_1}{1 - G_5} \tag{97}$$

$$\bar{N}_4 = \frac{G_3 G_4 \nabla G_1 - G_4 G_1 \nabla G_3}{1 - G_5} \tag{98}$$

$$\bar{N}_5 = \frac{G_2 G_3 \nabla G_5 - G_3 G_5 \nabla G_2 - G_2 G_5 \nabla G_3}{1 - G_5} - \frac{G_2 G_3 G_5 \nabla G_5}{(1 - G_5)^2} \tag{99}$$

$$\bar{N}_6 = \frac{G_3 G_4 \nabla G_5 - G_4 G_5 \nabla G_3 - G_3 G_5 \nabla G_4}{1 - G_5} - \frac{G_3 G_4 G_5 \nabla G_5}{(1 - G_5)^2} \tag{100}$$

$$\bar{N}_7 = \frac{G_4 G_1 \nabla G_5 - G_1 G_5 \nabla G_4 - G_4 G_5 \nabla G_1}{1 - G_5} - \frac{G_4 G_1 G_5 \nabla G_5}{(1 - G_5)^2} \tag{101}$$

$$\bar{N}_8 = \frac{G_1 G_2 \nabla G_5 - G_2 G_5 \nabla G_1 - G_1 G_5 \nabla G_2}{1 - G_5} - \frac{G_1 G_2 G_5 \nabla G_5}{(1 - G_5)^2} \tag{102}$$

The curls of the edge basis functions are given by

$$\nabla\times\bar{N}_5 = \frac{2(G_2\hat{n}_1 + G_3\hat{n}_4)}{1 - G_5} \tag{103}$$

$$\nabla\times\bar{N}_6 = \frac{2(G_3\hat{n}_3 + G_4\hat{n}_1)}{1 - G_5} \tag{104}$$

$$\nabla\times\bar{N}_7 = \frac{2(G_4\hat{n}_2 + G_1\hat{n}_3)}{1 - G_5} \tag{105}$$

$$\nabla\times\bar{N}_8 = \frac{2(G_1\hat{n}_4 + G_2\hat{n}_2)}{1 - G_5} \tag{106}$$

$$\nabla\times\bar{N}_1 = 0.5\nabla\times\bar{N}_8 + \hat{n}_6 \tag{107}$$

$$\nabla\times\bar{N}_2 = 0.5\nabla\times\bar{N}_6 + \hat{n}_8 \tag{108}$$

$$\nabla\times\bar{N}_3 = 0.5\nabla\times\bar{N}_5 + \hat{n}_7 \tag{109}$$

$$\nabla\times\bar{N}_4 = 0.5\nabla\times\bar{N}_7 + \hat{n}_5 \tag{110}$$

where the $\hat{n}_i$ are unit vectors in the direction of each master pyramid edge.

3.5.5 Face-based Vector Basis Functions for Pyramids

Consistent with Figure 4 , the face basis functions for pyramids are given by [9]

$$\bar{N}^f_1 = G_1\hat{n}_4 - G_2\hat{n}_1 - (1 - G_5)\hat{n}_6 \tag{111}$$

$$\bar{N}^f_2 = 0.5\left(G_5\hat{n}_5 + \frac{G_1G_5\hat{n}_3}{1 - G_5} - \left(2 - G_4 - \frac{G_4}{1 - G_5}\right)\hat{n}_2\right) \tag{112}$$

$$\bar{N}^f_3 = 0.5\left(G_5\hat{n}_6 + \frac{G_2G_5\hat{n}_2}{1 - G_5} - \left(2 - G_1 - \frac{G_1}{1 - G_5}\right)\hat{n}_4\right) \tag{113}$$

$$\overline{N^f}_4 = 0.5\left(G_5\hat{n}_7 + \frac{G_3 G_5 \hat{n}_4}{1 - G_5} - \left(2 - G_2 - \frac{G_2}{1 - G_5}\right)\hat{n}_1 \right) \tag{114}$$

$$\overline{N^f}_5 = 0.5\left(G_5\hat{n}_8 + \frac{G_4 G_5 \hat{n}_1}{1 - G_5} - \left(2 - G_3 - \frac{G_3}{1 - G_5}\right)\hat{n}_3 \right) \tag{115}$$

3.5.6 Edge-based Vector Basis Functions for Hexahedra

Like the tetrahedron and pyramid, the arbitrary hexahedral element is transformed to the master hexahedron as shown in Figure 5 . The assumed edge and face orientations are also shown in Figure 5 for edges E1-E12 and faces F1-F6.

The edge-based master basis functions for the hexahedron may be written in the following form [11]:

for edges || ξ,

$$\bar{N}_i = \frac{1}{8}(1 + \eta_i\eta)(1 + \zeta_i\zeta)\nabla\xi \tag{116}$$

for edges || η,

$$\bar{N}_i = \frac{1}{8}(1 + \xi_i\xi)(1 + \zeta_i\zeta)\nabla\eta \tag{117}$$

for edges || ζ,

$$\bar{N}_i = \frac{1}{8}(1 + \xi_i\xi)(1 + \eta_i\eta)\nabla\zeta \tag{118}$$

where (η_i, ζ_i) are the coordinate values of (η, ζ) on edge *i* and similarly for the other edges. These vector basis functions do guarantee tangential field continuity across element edges and faces, but are not divergence-free as are those for the tetrahedron. If, however, the hexahedral element is not distorted but is a rectangular brick, the basis functions are indeed divergence-free. EMPHASIS's use of hexahedral elements will, in fact, be only in the hybrid-mesh transition region where they will be rectangular bricks.

The curls of the edge basis functions are

for edges || ξ,

$$\nabla\times\bar{N}_i = \frac{1}{8}(1 + \eta_i\eta)\zeta_i\nabla\zeta\times\nabla\xi + \frac{1}{8}(1 + \zeta_i\zeta)\eta_i\nabla\eta\times\nabla\xi \tag{119}$$

for edges || η,

$$\nabla\times\bar{N}_i = \frac{1}{8}(1 + \xi_i\xi)\zeta_i\nabla\zeta\times\nabla\eta + \frac{1}{8}(1 + \zeta_i\zeta)\xi_i\nabla\xi\times\nabla\eta \tag{120}$$

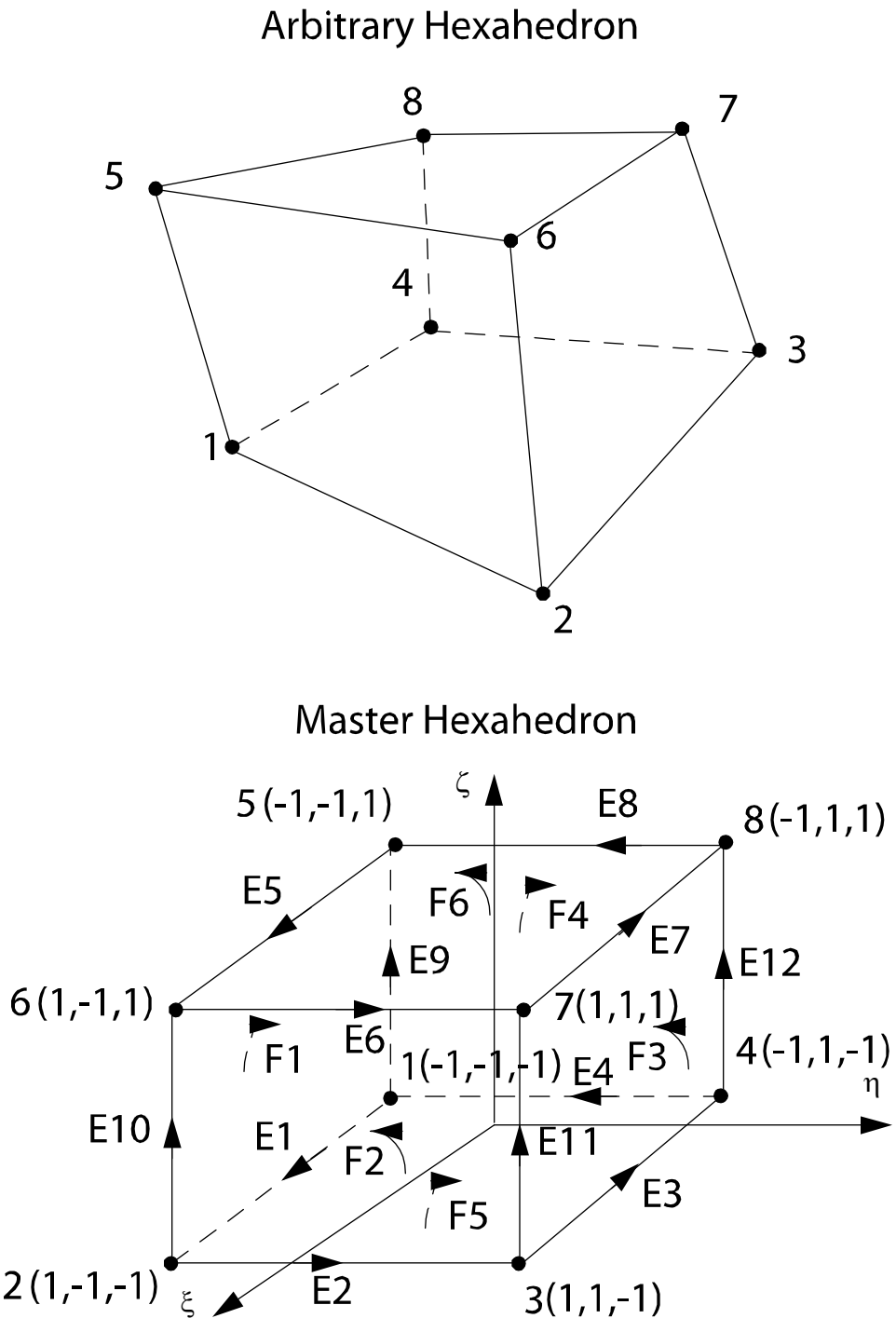

Figure 5 . Vector hexahedral element.

for edges || ζ,

$$\nabla\times\bar{N}_i = \frac{1}{8}(1+\xi_i\xi)\eta_i\nabla\eta\times\nabla\zeta + \frac{1}{8}(1+\eta_i\eta)\xi_i\nabla\xi\times\nabla\zeta \tag{121}$$

Note that the terms in these curl expressions are, in fact, the face basis functions given in the following section and therefore can be obtained from them.

3.5.7 Face-based Vector Basis Functions for Hexahedra

Consistent with Figure 5 , the face basis functions for hexahedra are given by

$$\bar{N}^f_1 = \frac{1}{8}(1+\eta_i\eta)(\nabla\xi\times\nabla\zeta) \tag{122}$$

$$\bar{N}^f_2 = \frac{1}{8}(1+\xi_i\xi)(\nabla\eta\times\nabla\zeta) \tag{123}$$

$$\bar{N}^f_3 = \frac{1}{8}(1+\eta_i\eta)(\nabla\zeta\times\nabla\xi) \tag{124}$$

$$\bar{N}^f_4 = \frac{1}{8}(1+\xi_i\xi)(\nabla\zeta\times\nabla\eta) \tag{125}$$

$$\bar{N}^f_5 = \frac{1}{8}(1+\zeta_i\zeta)(\nabla\eta\times\nabla\xi) \tag{126}$$

$$\bar{N}^f_6 = \frac{1}{8}(1+\zeta_i\zeta)(\nabla\xi\times\nabla\eta) \tag{127}$$

where the ξ_i, η_i, ζ_i are the coordinate values of ξ, η, ζ for the appropriate face, i.e., face 1 is in the (ξ, ζ) plane and η_i is its location in the η direction, etc.

3.6 Elemental Integral Evaluation for FEM Solution

Although for tetrahedra the elemental integrals in equations (15) and (64)-(66) can be evaluated analytically, instead the Jacobian transformation is used to transform all integrals to local coordinates on the master element. Integrals are then always performed on this master element using gaussian quadrature, simplifying and generalizing the code. This becomes very helpful when other elements are desired, such as pyramids and hexahedra, because the integrals cannot be done analytically on these elements. There is little or no time penalty in doing all integrations numerically because often the analytic expressions are themselves complicated and require many floating point operations to

complete. There is no accuracy penalty because by choosing the correct number of gauss points, the integrals are exact for the polynomial basis functions of interest here.

For the aforementioned elemental integrals, three forms are required

$$E_{ij} = \int_{\Omega e} \nabla\times\overline{W}_i \bullet \nabla\times\overline{W}_j dv \tag{128}$$

$$F_{ij} = \int_{\Omega e} \overline{W}_i \bullet \overline{W}_j dv \tag{129}$$

$$L_{ij} = \oint_{S} \hat{n}\times\overline{W}_i \bullet \hat{n}\times\overline{W}_j dS \tag{130}$$

Transforming to the master element, these become, using equations (83), (84), and (85),

$$E_{ij} = \int_{\tilde{\Omega}e} ([\boldsymbol{J}]^{-1}\tilde{\nabla}G_{i1}\times[\boldsymbol{J}]^{-1}\tilde{\nabla}G_{i2}) \bullet ([\boldsymbol{J}]^{-1}\tilde{\nabla}G_{j1}\times[\boldsymbol{J}]^{-1}\tilde{\nabla}G_{j2}) det([\boldsymbol{J}]) d\tilde{v} \tag{131}$$

$$F_{ij} =$$

$$\int_{\tilde{}} (G_{i1}[\boldsymbol{J}]^{-1}\tilde{\nabla}G_{i2} - G_{i2}[\boldsymbol{J}]^{-1}\tilde{\nabla}G_{i1}) \bullet (G_{j1}[\boldsymbol{J}]^{-1}\tilde{\nabla}G_{j2} - G_{j2}[\boldsymbol{J}]^{-1}\tilde{\nabla}G_{j1}) det([\boldsymbol{J}]) d\tilde{v} \tag{132}$$

$$\begin{aligned} L_{ij} = \int_{Se} & (\hat{n}_s \times (G_{i1}[\boldsymbol{J}_s]^{-1}\tilde{\nabla}G_{i2} - G_{i2}[\boldsymbol{J}_s]^{-1}\tilde{\nabla}G_{i1})) \bullet \\ & (\hat{n}_s \times (G_{j1}[\boldsymbol{J}_s]^{-1}\tilde{\nabla}G_{j2} - G_{j2}[\boldsymbol{J}_s]^{-1}\tilde{\nabla}G_{j1})) det([\boldsymbol{J}_s]) dS_e \end{aligned} \tag{133}$$

where in equation (133), the surface S is made up of those element faces where the term applies, $[J_s]$ is the Jacobian with respect to that surface, and $\hat{n}_s$ is the normal to the surface. The remaining term in equation (15) can be evaluated similarly,

$$\int_{\Omega e} \mu_0 \overline{W}_i \bullet \frac{\partial}{\partial t}\bar{J} dv = \mu_0 \int_{\Omega e} \left(([\boldsymbol{J}]^{-1}\tilde{\nabla}G_{i1}\times[\boldsymbol{J}]^{-1}\tilde{\nabla}G_{i2}) \bullet \frac{\partial}{\partial t}\bar{J} \right) det([\boldsymbol{J}]) d\tilde{v} \tag{134}$$

3.7 Wires

3.7.1 Transmission-line Model

The sub-cell modeling of wires generalizes a well-known finite-difference, transmission-line scheme [12]. The basic, 1-D transmission-line equations applied to the wire are

$$\frac{\partial I}{\partial l} = - C_w \frac{\partial V}{\partial t} - \frac{\sigma}{\varepsilon} C_w V \tag{135}$$

$$\frac{\partial V}{\partial l} = - L_w \frac{\partial I}{\partial t} + \bar{E}^t \bullet \hat{l} + \frac{1}{l}(V^{inc} - IR_w) \tag{136}$$

where I is the wire current, V is the wire voltage defined in the transmission-line sense (across the "line"), C_w is the capacitance per unit length of the wire, L_w is the inductance per unit length of the wire, both defined in the transmission-line sense, σ and ε are the conductivity and permittivity, respectively, of the medium surrounding the wire, $\bar{E}^t$ is the electric field driving the wire, V^{inc} is an applied voltage source on the wire, and R_w is a discrete resistor on the wire.

Taking the partial derivative of equation (135) with respect to l and substituting equation (136) yields the following 2nd order form:

$$\begin{aligned} L_w C_w \frac{d^2 I}{dt^2} + \left(L_w C_w \frac{\sigma}{\varepsilon} + \frac{R_w}{l} C_w \right) \frac{\partial I}{\partial t} - \frac{d^2 I}{dl^2} + C_w \frac{\sigma R_w}{\varepsilon l} I = \\ C_w \frac{\partial}{\partial t} \left(\bar{E}^t \bullet \hat{l} + \frac{V^{inc}}{l} \right) + C_w \frac{\sigma}{\varepsilon} \left(\bar{E}^t \bullet \hat{l} + \frac{V^{inc}}{l} \right) = f \end{aligned} \tag{137}$$

3.7.2 Finite-Element Solution

Applying Galerkin's method of weighted residual, where

$$r = - \frac{\partial}{\partial l} \left(\frac{\partial I}{\partial l} \right) + L_w C_w \frac{d^2 I}{dt^2} + \left(L_w C_w \frac{\sigma}{\varepsilon} + \frac{R_w}{l} C_w \right) \frac{\partial I}{\partial t} + C_w \frac{\sigma R_w}{\varepsilon l} I - f \tag{138}$$

and the weighted residual for wire element e is

$$\begin{aligned} R^e{}_i = \int_{\Omega e} (W_i \cdot r) dv = \\ \int_{\Omega e} \left(\left(\frac{\partial W_i}{\partial l} \frac{\partial I}{\partial l} - W_i \frac{\partial I}{\partial l} \Big|_{x1}^{x2} \right) + L_w C_w W_i \frac{d^2 I}{dt^2} + \left(L_w C_w \frac{\sigma}{\varepsilon} + \frac{R_w}{l} C_w \right) W_i \frac{\partial I}{\partial t} + C_w \frac{\sigma R_w}{\varepsilon l} W_i I - W_i f \right) dv \end{aligned} \tag{139}$$

where the first term has been integrated by parts. Setting the trial functions equal to the weighting functions, with

$$I = \sum_{i=1}^{2} W_j I_j \tag{140}$$

and setting the weighted residual to zero yields the following system

$$\begin{aligned}&\left[L_w C_w \int_{\Omega e} W_i W_j dv\right]\frac{d^2 I}{dt^2} + \left[\left(L_w C_w \frac{\sigma}{\varepsilon} + \frac{R_w}{l} C_w\right) \int_{\Omega e} W_i W_j dv\right]\frac{\partial I}{\partial t} + \\ &\left[C_w \frac{\sigma R_w}{\varepsilon l} \int_{\Omega e} W_i W_j dv + \int_{\Omega e} \frac{\partial W_i}{\partial l}\frac{\partial W_j}{\partial l} dv\right] I - \int_{\Omega e} W_i f dv = 0\end{aligned} \tag{141}$$

where I is the coefficient vector and the second term, $W_i \frac{\partial I}{\partial l}\Big|_{x1}^{x2}$, from the integration by parts has been discarded because it vanishes everywhere except at a boundary (end of wire), where there it also vanishes either because either a Dirichlet boundary condition ($I = 0$) or a Neumann boundary condition ($\partial I / \partial l = 0$) is applied there [13].

Applying a centered-difference approximation for the time derivatives yields the following,

$$\begin{aligned}&\left\{L_w C_w + L_w C_w \frac{\sigma \Delta t}{2\varepsilon} + \frac{R \Delta t}{2l} C_w\right\}[T] I^{n+\frac{3}{2}} = \\ &\left\{\left(2L_w C_w - \Delta t^2 C_w \frac{\sigma R}{\varepsilon l}\right)[T] - \Delta t^2 [S]\right\} I^{n+\frac{1}{2}} + \\ &\left\{\frac{\Delta t}{2}\left(L_w C_w \frac{\sigma}{\varepsilon} + \frac{R}{l} C_w\right) - L_w C_w\right\}[T] I^{n-\frac{1}{2}} + \Delta t^2 [F]\end{aligned} \tag{142}$$

where the elemental [T], [S], and [F] matrices are derived as follows. The linear, 1-D expansion functions are

$$W_1(l) = \frac{x_2^e - l}{l^e} \tag{143}$$

$$W_2(l) = \frac{l - x_1^e}{l^e} \tag{144}$$

where x_1^e and x_2^e are the local element endpoints and l^e is the element length. Using simple two-point trapezoidal integration,

$$\int_0^l f(x)dx = \frac{l}{2}(f(l) + f(0)) \tag{145}$$

the elemental matrices become

$$[T] = \begin{bmatrix} \int_{x1}^{x2} W_1 W_1 dl & \int_{x1}^{x2} W_1 W_2 dl \\ \int_{x1}^{x2} W_2 W_1 dl & \int_{x1}^{x2} W_2 W_2 dl \end{bmatrix} = \frac{l_e}{2}\begin{bmatrix} 1 & 0 \\ 0 & 1 \end{bmatrix} \tag{146}$$

$$[S] = \begin{bmatrix} \int_{x1}^{x2} \frac{\partial W_1}{\partial l}\frac{\partial W_1}{\partial l} dl & \int_{x1}^{x2} \frac{\partial W_1}{\partial l}\frac{\partial W_2}{\partial l} dl \\ \int_{x1}^{x2} \frac{\partial W_2}{\partial l}\frac{\partial W_1}{\partial l} dl & \int_{x1}^{x2} \frac{\partial W_2}{\partial l}\frac{\partial W_2}{\partial l} dl \end{bmatrix} = \frac{1}{l_e}\begin{bmatrix} 1 & -1 \\ -1 & 1 \end{bmatrix} \tag{147}$$

and

$$[F] = \begin{bmatrix} \int_{x1}^{x2} f W_1 dl \\ \int_{x1}^{x2} f W_2 dl \end{bmatrix} = f\frac{l_e}{2}\begin{bmatrix} 1 \\ 1 \end{bmatrix} \tag{148}$$

Note that the matrix to be inverted, [*T*], is diagonal so the solve is a direct one.

3.7.3 Implementation: Second-Order Formulation

Implementation of the sub-cell wire algorithm involves several heuristic techniques for evaluating the wire parameters and drive terms in equation (137). These include the wire inductance and capacitance per unit length, L_w and C_w, the permeability, permittivity, and conductivity surrounding the wire, μ, ε, σ, and the electric-field drive for the wire, $\bar{E}^t$.

The inductance per unit length for the wire is defined in a "coaxial" sense as

$$L_w = \frac{\bar{\mu}}{2\pi} \ln \frac{\bar{d}}{a} \tag{149}$$

where μ is an "average" permeability around the wire, $\bar{d}$ is an "average" distance between the wire and its "driving elements", and *a* is the wire radius. Similarly, the capacitance per unit length for the wire is defined as

$$C_w = \frac{2\pi\varepsilon}{\ln \frac{\bar{d}}{a}} \tag{150}$$

where $\bar{\varepsilon}$ is an "average" permittivity around the wire. These quantities are defined for each segment of the wire as the wire passes through an arbitrary mesh topology.

The "driving elements" for the wire are those elements surrounding the wire path which are "1 cell distant" from the wire. In other words, those elements which connect to nodes which connect to wire nodes through an element edge, EXCEPT for those nodes OR elements touching the wire. In this way, an annulus of elements is defined surrounding but not touching the wire which supply the drive.

The "driving elements" are also used to compute the "average" distance $\bar{d}$ in the following manner: Define a wire-current direction at each wire node, $\hat{l}_i$, as the unit vector connecting the mid-points of the two edges connected to the wire node. If the wire node is an end node, take the direction of the end edge as the wire-current direction. Also define a vector for each "driving element" from the wire node to the center of the driving element, $\bar{\xi}_k$ The "nodal average" distance is then defined as

$$\bar{d}^n{}_i = \frac{1}{N_i} \sum_{k=1}^{N_i} \left| \hat{l}_i \times \bar{\xi}_k \right| \tag{151}$$

where N_i is the number of driving elements for node *i*. The average distance used in equations (149) and (150) is from the wire segment, defined for the k^{th} segment as

$$\bar{d}_k = (\bar{d}_i^n + \bar{d}_j^n) \tag{152}$$

where $\bar{d}^n{}_i$ and $\bar{d}^n{}_j$ are the "nodal average" distances from the nodes at the ends of the k^{th} segment.

The "average" permeability, permittivity, and conductivity surrounding the wire, $\bar{\mu}$, $\bar{\varepsilon}$, and $\bar{\sigma}$ are computed by simply summing these parameters for each element connected to the wire edge of interest and dividing by the number of these connected elements.

The explicit solve for advancing the wire current to $I^{n+3/2}$ in equation (142) is centered at time *n + 1/2*. Therefore, the electric-field drive for the wire should be centered there as well. This requires backstoring of the electric field for one cycle, leading to the following expressions for the drive terms in equation (137):

$$\frac{\partial \bar{E}^t}{\partial t} = \frac{\bar{E}^{n+1} - \bar{E}^n}{\Delta t} \tag{153}$$

$$\bar{E}^t = \frac{\bar{E}^{n+1} + \bar{E}^n}{2} \tag{154}$$

where $\bar{E}^{n+1}$ and $\bar{E}^n$ are the average of the barycenter electric field over all of the "driving elements" at time *n + 1* (most recent) and *n* (next-most recent), respectively. Since the driving elements are associated with wire nodes, the values for the end nodes of each wire segment are spatially averaged to obtain the final electric field drives for the wire segments used in equations (137) and (142).

The wire current is injected back into the volume field solution through the normal Maxwell current-source term from equation (6),

$$-\mu_0 \frac{\partial}{\partial t} \bar{J} \tag{155}$$

3.7.4 Implementation: First-Order Formulation

Wires have not yet been implemented for the first-order formulation.

3.7.5 Unconditionally Stable Modifications

The wire formulation described previously is conditionally stable and will consequently limit the size of the time step to the Courant step derived from the wire discretization.

An unconditionally stable formulation is described in [14] and it's references. This formulation creates a tighter and symmetric coupling between the wire and the field drives.

This formulation alters the form of the wire-drive term *f* in equations (137)-(139) and the corresponding volumetric field drive term in equations (15)-(18). For the wire drive, weak form,

$$\int_{\Omega e} W_i f dv = \int_{\Omega e} W_i \left(\frac{C_w}{l} \frac{\partial V^{inc}}{\partial t} + \frac{C_w}{l} \frac{\sigma}{\varepsilon} V^{inc} \right) dv + \int_{\Omega e} g(r) W_i \left(C_w \frac{\partial}{\partial t} (\bar{E}^t \bullet \hat{l}) + C_w \frac{\sigma}{\varepsilon} (\bar{E}^t \bullet \hat{l}) \right) dv \tag{156}$$

where $g(r)$ is a radial weighting function around the wire such that

$$\int_{r \geq a} 2\pi r g(r) dr = 1 \tag{157}$$

where a is the wire radius and

$$g(r) = 0. \tag{158}$$

for $r < a$ and $r > d$. For $a < r < d$,

$$g(r) = \frac{1 + \cos\left(\pi \frac{r}{d}\right)}{\pi(d^2 - a^2) - 2\frac{d^2}{\pi}\left(1 + \cos\left(\pi \frac{a}{d}\right) + \pi \frac{a}{d} \sin\left(\pi \frac{a}{d}\right)\right)} \tag{159}$$

Expanding the electric field as before

$$\bar{E} = \sum_{j=1}^{m} \bar{N}_j E_j \tag{160}$$

the second term in the right-hand side of equation (156) becomes

$$\sum_{j=1}^{m} \left[\frac{\partial E_j}{\partial t} \int_{\Omega e} C_w \bar{N}_j \bullet \hat{l} g(r) W_i dv + \bar{E}_j \int_{\Omega e} C_w \frac{\sigma}{\varepsilon} \bar{N}_j \bullet \hat{l} g(r) W_i dv \right] \tag{161}$$

For the field drive,

$$\int_{\Omega e} \mu_0 \bar{N}_i \bullet \frac{d}{dt} \bar{J} dv \tag{162}$$

the current density from the wire is written as

$$\bar{J}(\bar{r}, t) = I(s, t) g(r) \hat{l} \tag{163}$$

Using the expansion in equation (140) for I,

$$\bar{J}(\bar{r}, t) = \sum_{j=1}^{\angle} W_j(l) g(r) I_j(t) I(s, t) \hat{l} \tag{164}$$

so equation (162) becomes

$$\mu_0 \sum_{j=1}^{\angle} \frac{\partial}{\partial t} I_j(t) \int_{\Omega e} W_j(l) g(r) \bar{N}_i(\bar{r}) \bullet \hat{l} dv$$

(165)

Note the similarities between equation (161) and equation (165). The volume integral over the element is the same and in the first term of equation (161) the derivative operates on edge projection E_j or wire current I_j, respectively. This suggests that now the wire currents at the wire nodes should be included in the edge unknown system and solved simultaneously. The following coupled system represents this,

$$\begin{bmatrix} [T] & 0 \\ 0 & [T_w] \end{bmatrix} \frac{d^2}{dt^2} \begin{bmatrix} E \\ I \end{bmatrix} + \begin{bmatrix} [B] & \mu_0 [P_w]^T \\ -C_w [P_w] & [B_w] \end{bmatrix} \frac{\partial}{\partial t} \begin{bmatrix} E \\ I \end{bmatrix} + \begin{bmatrix} [S] & 0 \\ -C_w \frac{\sigma}{\varepsilon} [P_w] & [S_w] \end{bmatrix} \begin{bmatrix} E \\ I \end{bmatrix} + \begin{bmatrix} F_e \\ F_w \end{bmatrix} = 0 \tag{166}$$

where

$$P_{w,ij} = \int_{\Omega e} W_j(l) g(r) \bar{N}_i(\bar{r}) \bullet \hat{l} dv \tag{167}$$

$$F_w = -\int_s W_i \left(\frac{C_w}{l} \frac{\partial V^{inc}}{\partial t} + \frac{C_w}{l} \frac{\sigma}{\varepsilon} V^{inc} \right) ds \tag{168}$$

3.7.6 Finite-Element Solution

From equation (166), dividing thru by C_w, the coupled wire equation is

$$[T_w]\ddot{I} - [P_w]\dot{E} + [B_w]\dot{I} - \frac{\sigma}{\varepsilon}[P_w]E + [S_w]I + [F_w] = 0 \tag{169}$$

where

$$[T_w] = L_w \int_{\Omega e} W_i W_j dv \tag{170}$$

$$[B_w] = \left(L_w \frac{\sigma}{\varepsilon} + \frac{R_w}{l} \right) \int_{\Omega e} W_i W_j dv \tag{171}$$

$$[S_w] = \frac{\sigma R_w}{\varepsilon l} \int_{\Omega e} W_i W_j dv + \frac{1}{C_w} \int_{\Omega e} \frac{\partial W_i}{\partial l} \frac{\partial W_j}{\partial l} dv \tag{172}$$

$$[F_w] = \int_{\Omega e} W_i \left(\frac{\partial}{\partial t} \left(\frac{V^{inc}}{l} \right) + \frac{\sigma}{\varepsilon} \left(\frac{V^{inc}}{l} \right) \right) dv \tag{173}$$

$$[P_w] = \int_{\Omega e} W_j(l) g(r) \overline{N}_i(\bar{r}) \bullet \hat{l} \, dv \tag{174}$$

Using Newmark approximations,

$$T_w \left(\frac{I^{n+1} - 2I^n + I^{n-1}}{\Delta t^2} \right) - P_w \left(\frac{E^{n+1} - E^{n-1}}{2\Delta t} \right) + B_w \left(\frac{I^{n+1} - I^{n-1}}{2\Delta t} \right) - \frac{\sigma}{\varepsilon} P_w \left(\frac{E^{n+1} + 2E^n + E^{n-1}}{4} \right) + S_w \left(\frac{I^{n+1} + 2I^n + I^{n-1}}{4} \right) + F_w = 0 \tag{175}$$

$$\left(4T_w + 2\Delta t B_w + \Delta t^2 S_w \right) I^{n+1} + \left(-8T_w + 2\Delta t^2 S_w \right) I^n + \left(4T_w - 2\Delta t B_w + \Delta t^2 S_w \right) I^{n-1} - \left(2\Delta t P_w + \Delta t^2 \frac{\sigma}{\varepsilon} P_w \right) E^{n+1} = 2\Delta t^2 \frac{\sigma}{\varepsilon} P_w E^n - \left(2\Delta t P_w - \Delta t^2 \frac{\sigma}{\varepsilon} P_w \right) E^{n-1} - 4\Delta t^2 F_w \tag{176}$$

$$\left(4T_w + 2\Delta t B_w + \Delta t^2 S_w \right) I^{n+1} - \left(2\Delta t P_w + \Delta t^2 \frac{\sigma}{\varepsilon} P_w \right) E^{n+1} = \left(8T_w - 2\Delta t^2 S_w \right) I^n + 2\Delta t^2 \frac{\sigma}{\varepsilon} P_w E^n - \left(4T_w - 2\Delta t B_w + \Delta t^2 S_w \right) I^{n-1} - \left(2\Delta t P_w - \Delta t^2 \frac{\sigma}{\varepsilon} P_w \right) E^{n-1} - 4\Delta t^2 F_w \tag{177}$$

$$A_w I^{n+1} = b_w + \left(2\Delta t P_w + \Delta t^2 \frac{\sigma}{\varepsilon} P_w \right) E^{n+1} \tag{178}$$

$$I^{n+1} = A_w^{-1} \left(b_w + \left(2\Delta t P_w + \Delta t^2 \frac{\sigma}{\varepsilon} P_w \right) E^{n+1} \right) \tag{179}$$

where b_w is the right hand side of equation (177) and

$$A_w = 4T_w + 2\Delta t B_w + \Delta t^2 S_w \tag{180}$$

Also from equation (166), the coupled field equations are

$$[T]\ddot{E} + [B]\dot{E} + \mu_0 [P_w]^T \dot{I} + [S]E + [F_e] = 0 \tag{181}$$

Again with Newmark approximations,

$$T\left(\frac{E^{n+1} - 2E^n + E^{n-1}}{\Delta t^2}\right) + B\left(\frac{E^{n+1} - E^{n-1}}{2\Delta t}\right) + \mu_0 P_w^T\left(\frac{I^{n+1} - I^{n-1}}{2\Delta t}\right) + S\left(\frac{E^{n+1} + 2E^n + E^{n-1}}{4}\right) + F_e = 0 \tag{182}$$

$$\begin{aligned} &\left(4T + 2\Delta t B + \Delta t^2 S\right)E^{n+1} + 2\Delta t \mu_0 P_w^T I^{n+1} = \\ &\left(8T - 2\Delta t^2 S\right)E^n - \left(4T - 2\Delta t B + \Delta t^2 S\right)E^{n-1} + 2\Delta t \mu_0 P_w^T I^{n-1} - 4\Delta t^2 F_e = b \end{aligned} \tag{183}$$

$$\begin{aligned} &\left(4T + 2\Delta t B + \Delta t^2 S\right)E^{n+1} + 2\Delta t \mu_0 P_w^T I^{n+1} = \\ &2\left(4T + 2\Delta t B + \Delta t^2 S\right)E^n - 4\Delta t^2 S E^n - 4\Delta t B E^n - \left(4T + 2\Delta t B + \Delta t^2 S\right)E^{n-1} + \\ &4\Delta t B E^{n-1} + 2\Delta t \mu_0 P_w^T I^{n-1} - 4\Delta t^2 F_e = b \end{aligned} \tag{184}$$

Further manipulation of equation (184) produces an equation similar to equation (18),

$$\left(4T + 2\Delta t B + \Delta t^2 S\right)E^{n+1} - 2\left(4T + 2\Delta t B + \Delta t^2 S\right)E^n + \left(4T + 2\Delta t B + \Delta t^2 S\right)E^{n-1} + 2\Delta t \mu_0 P_w^T I^{n+1} = -4\Delta t(B + \Delta t S)E^n + 4\Delta t B E^{n-1} + 2\Delta t \mu_0 P_w^T I^{n-1} - 4\Delta t^2 F_e = b \tag{185}$$

$$\begin{aligned} &A(E^{n+1} - 2E^n + E^{n-1}) + 2\Delta t \mu_0 P_w^T I^{n+1} = A\hat{E} + 2\Delta t \mu_0 P_w^T I^{n+1} = \\ &(-4\Delta t(B + \Delta t S)E^n + 4\Delta t B E^{n-1} + 2\Delta t \mu_0 P_w^T I^{n-1} - 4\Delta t^2 F_e = b \end{aligned} \tag{186}$$

Substituting for I^{n+1},

$$A\hat{E} + 2\Delta t \mu_0 P_w^T\left(A_w^{-1}\left(b_w + \left(2\Delta t P_w + \Delta t^2 \frac{\sigma}{\varepsilon} P_w\right)\left(\hat{E} + 2E^n - E^{n-1}\right)\right)\right) = b \tag{187}$$

where

$$A = 4T + 2\Delta t B + \Delta t^2 S \tag{188}$$

and

$$\hat{E} = E^{n+1} - 2E^n + E^{n-1} \tag{189}$$

Expanding equation (187),

$$A\hat{E} + 2\Delta t\mu_0 P_w^T A_w^{-1} b_w + 4\Delta t^2 \mu_0 P_w^T A_w^{-1} P_w \hat{E} + 2\Delta t^3 \mu_0 P_w^T A_w^{-1} \frac{\sigma}{\varepsilon} P_w \hat{E} + 4\Delta t^2 \mu_0 P_w^T A_w^{-1} P_w \left(2E^n - E^{n-1}\right) + 2\Delta t^3 \mu_0 P_w^T A_w^{-1} \frac{\sigma}{\varepsilon} P_w \left(2E^n - E^{n-1}\right) = b \tag{190}$$

$$A\hat{E} + 2\Delta t\mu_0 P_w^T A_w^{-1} b_w + 2\Delta t^2 \mu_0 P_w^T A_w^{-1} (2P_w + \Delta t \frac{\sigma}{\varepsilon} P_w)\hat{E} + 2\Delta t^2 \mu_0 P_w^T A_w^{-1} (2P_w + \Delta t \frac{\sigma}{\varepsilon} P_w)\left(2E^n - E^{n-1}\right) = b \tag{191}$$

$$\left(A + H\right)\hat{E} = b - 2\Delta t\mu_0 P_w^T A_w^{-1} b_w - 2\Delta t^2 \mu_0 P_w^T A_w^{-1}\left(2 + \Delta t \frac{\sigma}{\varepsilon}\right) P_w \left(2E^n - E^{n-1}\right) = b' \tag{192}$$

where

$$H = 2\Delta t^2 \mu_0 P_w^T A_w^{-1}\left(2 + \Delta t \frac{\sigma}{\varepsilon}\right) P_w \tag{193}$$

Equation (192) is now solved for $\hat{E}$, followed by the normal time advance computing E^{n+1}, which is substituted back into equation (179) to compute I^{n+1}.

The desired matrix solution method is conjugate gradient (CG), therefore, the solution to equation (192) can be accomplished in two steps knowing that CG will multiply vectors p by $A + H$,

$$A_w q = P_w p \tag{194}$$

$$\left(A + H\right)p = Ap + 2\Delta t^2 \mu_0 P_w^T \left(2 + \Delta t \frac{\sigma}{\varepsilon}\right) q \tag{195}$$

In this manner, the matrix solution can be obtained without computing H directly. For multiple wires, the field equations become

$$[T]\ddot{E} + [B]\dot{E} + \mu_0 [P_{w1}]^T \dot{I}_1 + \mu_0 [P_{w2}]^T \dot{I}_2 + ... + [S]E + [F_e] = 0 \tag{196}$$

For two wires,

$$\left(4T + 2\Delta tB + \Delta t^2 S\right)E^{n+1} + 2\Delta t\mu_0 \left(P_{w1}^T I_1^{n+1} + P_{w2}^T I_2^{n+1}\right) = \left(8T - 2\Delta t^2 S\right)E^n - \left(4T - 2\Delta tB + \Delta t^2 S\right)E^{n-1} + 2\Delta t\mu_0 \left(P_{w1}^T I_1^{n-1} + P_{w2}^T I_2^{n-1}\right) - 4\Delta t^2 F_e = b \tag{197}$$

Substituting for I^{n+1},

$$AE^{n+1} + 2\Delta t\mu_0 P_{w1}^T A_{w1}^{-1} b_{w1} + 2\Delta t^2 \mu_0 P_{w1}^T A_{w1}^{-1} P_{w1}(2 + \Delta t\frac{\sigma}{\varepsilon})E^{n+1} + 2\Delta t\mu_0 P_{w2}^T A_{w2}^{-1} b_{w2} + 2\Delta t^2 \mu_0 P_{w2}^T A_{w2}^{-1} P_{w2}(2 + \Delta t\frac{\sigma}{\varepsilon})E^{n+1} = b \tag{198}$$

$$\left(A + H\right)E^{n+1} = b - 2\Delta t\mu_0 P_{w1}^T A_{w1}^{-1} b_{w1} - 2\Delta t\mu_0 P_{w2}^T A_{w2}^{-1} b_{w2} = b' \tag{199}$$

where now

$$H = 2\Delta t^2 \mu_0 \left(P_{w1}^T A_{w1}^{-1} P_{w1}\left(2 + \Delta t\frac{\sigma}{\varepsilon}\right) + P_{w2}^T A_{w2}^{-1} P_{w2}\left(2 + \Delta t\frac{\sigma}{\varepsilon}\right)\right) \tag{200}$$

Two solves are now required for q's,

$$A_{w1} q_1 = P_{w1} p \tag{201}$$

$$A_{w2} q_2 = P_{w2} p \tag{202}$$

then

$$\left(A + H\right)p = Ap + 2\Delta t^2 \mu_0 \left(2 + \Delta t\frac{\sigma}{\varepsilon}\right)P_{w1}^T q_1 + 2\Delta t^2 \mu_0 \left(2 + \Delta t\frac{\sigma}{\varepsilon}\right)P_{w2}^T q_2 \tag{203}$$

3.8 Slots

3.8.1 Transmission-line Model

The sub-cell slot model is the dual of the above wire formulation. The 1-D transmission line equations applied to the slot are

$$\frac{\partial I}{\partial l} = - C_s \frac{\partial V}{\partial t} - \frac{1}{l}[\bar{H}^{diff} \bullet \hat{l}] \tag{204}$$

$$\frac{\partial V}{\partial l} = - L_s \frac{\partial I}{\partial t} \tag{205}$$

where I is the slot "current", V is the slot "voltage" ("magnetic current"), C_s is the "capacitance" per unit length of the slot, L_s is the "inductance" per unit length of the slot, $\bar{H}^{diff}$ is the two-sided magnetic-field difference driving the slot, and $\hat{l}$ is the unit vector defining the slot-segment direction. These equations lead to the 2nd order form

$$L_s C_s \frac{d^2 V}{dt^2} - \frac{d^2 V}{dl^2} = \frac{L_s}{l}\frac{\partial}{\partial t}(\bar{H}^{diff} \bullet \hat{l}) = f$$

(206)

3.8.2 Finite-Element Solution

Applying Galerkin's method, expanding the unknown slot voltage as

$$V = \sum_{j=1}^{2} W_j V_j \tag{207}$$

and applying central differencing,

$$\{L_s C_s\}[T]V^{n+2} = \{2L_s C_s[T] - \Delta t^2[S]\}V^{n+1} - \{L_s C_s\}[T]V^n + \Delta t^2[F] \tag{208}$$

The remaining steps are identical to those for the wire, with the matrices [*T*], [*S*], and [*F*] being identical to those for the wire.

3.8.3 Implementation: Second-Order Formulation

Implementation of the sub-cell slot algorithm is in most ways the dual of the wire algorithm. However, the heuristic techniques for evaluating the parameters in equation (206) differ in many cases. These include the slot inductance and capacitance per unit length, L_s and C_s, the permeability and permittivity inside and surrounding the slot, μ, ε, and the magnetic-field drive for the wire, $\bar{E}^{diff}$. For the present formulation, the slot is assumed lossless and therefore the slot conductivity is not needed.

The inductance per unit length for the slot is defined in a "dual coaxial" sense as

$$L_s = \frac{\pi\mu}{2\ln\frac{\bar{d}}{a}} \tag{209}$$

where $\bar{\mu}$ is an "average" permeability around the slot, $\bar{d}$ is an "average" distance between the slot and its "driving elements", and a is the slot effective radius, which is a function of the slot width and depth [15]

$$a = \frac{width}{4} e^{-\frac{\pi \cdot depth}{2 \cdot width}} \tag{210}$$

Similarly, the capacitance per unit length for the slot is defined as

$$C_s = \frac{2\bar{\varepsilon}}{\pi}\ln\frac{\bar{d}}{a} \tag{211}$$

where $\bar{\varepsilon}$ is an "average" permittivity around the slot. These quantities are defined for each segment of the slot as it passes through an arbitrary mesh topology.

Unlike the wire, the "driving elements" for the slot include all elements immediately surrounding the slot including those which "touch" the slot. Also differing from the wire, two separate lists of driving elements must be kept for the slot. This is due to the fact that the "magnetic current" driving the slot is derived from the difference of the tangential magnetic fields on either side of the slot plane, which must be defined to be a perfect electrical conducting (PEC) plane in the FEM model. In order to facilitate the selection of the two drive "sides" of the slot, the material type of opposite sides of the slot PEC plane must be different.

The pseudo-PEC edges contributing the magnetic-current drive for the slot are those edges in the PEC plane connecting to a slot node. A list is also kept of these edges so that they may be reset in the FEM solution from their normal "set to zero" Dirichlet condition for a PEC to the appropriate slot-drive value.

Exactly like the wire, "slot-current" directions, $\hat{l}_i$, are defined at each node. Using these, sub-distances for each node are determined using equation (151) for each of the two "driving-element" lists at the node. These two equation (151) results are then averaged together to obtain the "nodal average" distance. The average distance relative to the slot segment needed in equations (209) and (211) is then determined as for the wire, from equation (152). Some special storage and communication is required for these operations to succeed in a distributed parallel computing environment.

The average permeability and permittivity around the slot are computed exactly like those for the wire.

The explicit solve for advancing the slot voltage to V^{n+2} in equation (208) is centered at time $n + 1$. Therefore, the magnetic-field drive for the slot should be centered there as well. The two-sided magnetic-field difference is obtained from the curl of the latest electric field using standard FEM interpolation. For each slot node, $\frac{\partial}{\partial t}\bar{H}$ is formed by averaging the barycenter $\frac{\partial}{\partial t}\bar{H}$ from the "driving elements" on each side of the slot plane. The two node contributions for each slot segment from each side are then averaged to form the total average $\frac{\partial}{\partial t}\bar{H}$ contribution from each side of the slot plane for each slot segment. Finally, the difference is taken between the $\frac{\partial}{\partial t}\bar{H}$'s from each side to form the total $\frac{\partial \bar{H}^{diff}}{\partial t}$ for each slot segment.

As alluded to earlier, the perturbation of the slot is fed back into the volume field solution by introducing the slot voltage into the volume solution as a Dirichlet boundary condition on the pseudo-PEC edges which surround the slot in the slot plane. This provides a "magnetic-current" drive, effectively providing a non-zero tangential electric field in an

otherwise PEC plane. This drive appears in Maxwell's equations as a fictitious magnetic-current source term, not shown in Section 2 of this document.

3.8.4 Implementation: First-Order Formulation

Slots have not yet been implemented for the first-order formulation.

3.9 Absorbing and Impedance Boundary Conditions

Absorbing or impedance boundary conditions are encompassed in the following term from equation (15),

$$\left[\oint_S \frac{1}{v_p \mu_r} \hat{n} \times \overline{W}_i \bullet \hat{n} \times \overline{W}_j dS\right] \frac{\partial E}{\partial t} \tag{212}$$

where the speed of light, c, has been replaced by v_p, the phase velocity in the material media of interest. The speed of light originally came from application of the Sommerfeld radiation condition, equation (11), applied to free space.

For application of a 1st order absorbing boundary condition,

$$\frac{1}{v_p \mu_r} = \frac{\sqrt{\mu\varepsilon}}{\mu_r} = c\sqrt{\frac{\varepsilon_r}{\mu_r}} \tag{213}$$

For application as an impedance boundary condition, since $Z = \sqrt{\frac{\mu}{\varepsilon}}$, the same is written

$$\frac{1}{v_p \mu_r} = \frac{\mu_0}{Z} \tag{214}$$

In free space, for example, a "matched" impedance condition is achieved with

$$Z = \sqrt{\frac{\mu_0}{\varepsilon_0}} \tag{215}$$

therefore

$$\frac{\mu_0}{Z} = c \tag{216}$$

so the absorbing condition is recovered from the impedance condition.

Absorbing and impedance boundary conditions are presently functional only for the second-order formulation.

3.10 Edge Loads

Edge loads are implemented in a somewhat ad-hoc manner using the expression for the contribution to the FEM system of a post with an impedance Z_L in Jin [16] whose matrix contribution for a single edge is of the form

$$\frac{jk_0 Z_0}{Z_L} \tag{217}$$

where Z_0 is the impedance of free space. For a single resistor R on a single element edge, the contribution is

$$\frac{j\omega Z_0}{cR} \tag{218}$$

where c is the speed of light. This term consequently contributes to the first-derivative term in equation (16) and consequently [B] in equation (18), both matrix and rhs, for that edge only.

Similarly, for a single inductor L, the contribution is

$$\frac{Z_0}{cL} \tag{219}$$

which contributes to the constant term [S] in equations (16) and (18), both matrix and rhs. For a single capacitor C, the contribution is

$$\frac{(j\omega)^2 Z_0}{c(1/C)} \tag{220}$$

contributing to the second-derivative term [T] in equations (16) and (18). Note that this term does not appear in the rhs, only in the matrix.

4.0 Verification

Verification determines whether the numerical model being implemented has been correctly coded. This normally consists of comparison with know analytic solutions requiring simple problems in separable geometries.

Since the unstructured FEM implementation of EMPHASIS within NEVADA closely follows the well-verified legacy code VOLMAX [17][18][19][20], the verification strategy for the basic electro-magnetics implementation is to make extremely detailed comparisons of EM simulations between the two codes. “Extremely detailed” means comparison of vector-field values, wire currents, and slot voltages down to near machine

precision. In this way, the argument is made that UTDEM is verified by extension of VOLMAX verification. For the 1.0 release of UTDEM, all algorithms were re-implementations of existing VOLMAX algorithms. Reference [21] provides a summary of the full VOLMAX verification suite.

New algorithms implemented subsequently into UTDEM must and have been verified separately. This includes verification directed toward fundamental application areas such as Box- and Cavity-SGEMP. A separate document covers the Cable-SGEMP application [22].

To this end, several problems have been compared in this manner ranging from simple rectangular cavities to complex, arbitrary shaped cavities including wires, slots, and lossy material. These are described in the following sections. The corresponding EMPHASIS/NEVADA input files are provided in the Appendix. These also happen to be included in the UTDEM regression-suite.

All of these verification problems exercise only the second-order formulation. The first-order formulation has not been fully integrated with the necessary ancillary tools and has not been fully exercised.

4.1 UCAVITY

This is a simple rectangular perfectly conducting cavity enclosure with free space inside, meshed using unstructured tetrahedra. The cavity is shaped somewhat like a shoe box. The source is a gaussian pulse applied directly to an electric-field edge projection interior to the cavity. The observer is another edge projection elsewhere in the cavity. This simulation tests the second-order formulation, the PEC boundary condition, the simple-electrical material model, and the simplest possible source and observer. Being careful to perfectly match the time steps between the two codes, the results agree with VOLMAX to machine precision.

4.2 UCAVABC

This is the same geometry, mesh, material, drive, and observer as for the above UCAVITY problem. The difference is the PEC boundary condition defining the cavity is replaced with a simple 1st order absorbing boundary condition (ABC). This simulation tests the ABC along with further testing of the second-order formulation, etc. These results also agree with VOLMAX to machine precision.

4.3 UCAVABC_2MAT_LOSS

This is the same geometry, mesh, drive, observer, and ABC outer boundary condition as the above UCAVABC problem except that two different materials now exist within the cavity enclosure. The source is in one material and the observer is in the other. The materials are no longer simply free space, but have relative permeabilities and relative permittivities different from unity and have non-zero conductivities. This simulation

further tests the simple-electrical material model and the implementation of material parameters and volumetric loss into the FEM solution. Again, the results agree with VOLMAX to machine precision.

4.4 UCAVABC_WIRE

This is the same geometry, drive, observer, and ABC as the UCAVABC problem above but with a different tetrahedral interior mesh. A thin wire has been added along the length of the cavity near the center of the cross section. This wire also has a wire current observer defined on it. The material inside the cavity is reverted to all free space.

This simulation tests the thin-wire algorithm along with further testing previously verified implementations of the second-order formulation, ABC, etc. Both the interior field observer and the wire current agree with VOLMAX to machine precision.

This simulation has also been run replacing the field source with a wire current source, also producing machine-precision agreement with VOLMAX.

4.5 UCAVABC_SLOTS

This problem consists of two concentric rectangular boxes, or “shoe box within a shoe box”. The interior box is a PEC boundary with two slots defined on two different sides of the box. This box contains the same source and observer as did the previous problems, but with a different tetrahedral mesh. The two slots have different widths, small fractions of a typical edge length. Both slots have zero depth. The outer box has an ABC on its surface, and an additional field observer is added between the two boxes. Slot voltage observers are located on each slot, and the material everywhere is free space.

With both slots activated, both field observers and both slot observers agree perfectly with VOLMAX. If the slots are deactivated, as expected only the observer inside the inner cavity is nonzero, the observer between the boxes is identically zero, again in agreement with VOLMAX.

4.6 UCOAX_BELT

This geometry consists of two concentric cylinders with end caps, representing a section of coaxial transmission line. The interior is meshed with unstructured tetrahedra, all with a relative permittivity of 2.2, relative permeability of unity, and zero conductivity. PEC boundary conditions exist on the cylinders and ABC’s exist on the two end caps. The source is a short, “delta-gap” type source on the surface of the inner cylinder near one of the end caps. This source launches a wave down the coaxial line in a relatively clean manner except very near the source. Observers are two line-integral voltage observers defined radially between the two cylinders, at two different points along the line length.

This problem tests implementations of the “belt” source on a surface and the line-integral voltage observers.

The simulation launches a short gaussian-shaped pulse down the line. This wave is detected by the two observer line integrals and agrees perfectly with VOLMAX. The ABC at the end of the line section does a good job of absorbing the pulse, preventing reflections. The simulation was also run with the ABC's replaced by PEC's. As expected, the pulse now reflects back and forth along the line "forever" since there is no loss.

Additional simulations were performed with the end-cap ABC's replaced by impedance boundary conditions (IBC's). Various values were tested including a "matched" condition, which reproduces the absorbing result exactly.

5.0 Validation

Validation determines whether the model being implemented correctly reproduces real physical phenomena for a specific application. This normally consists of comparison with carefully designed experiments to examine specific aspects of the code or with other trusted experimental results.

The legacy code VOLMAX, the origin of all of the algorithms described in this document, is also well validated against published experiments, analytical, and numerical results [17][18][19][20]. These include scattering from a perfectly conducting sphere, resonances of a cylindrical cavity, scattering from a thin wire, input admittance of a loop antenna modeled by a thin wire [17], excitation of loaded thin wires in cavities with thin slots [18], gas-discharge excitation of conical transmission-line antennas [19], and more loaded wires in cavities with slots [20]. Therefore, similar to verification, an argument can be made that UTDEM is validated by implication from VOLMAX validation. Reference [21] provides a summary of the full VOLMAX validation suite. New applications for UTDEM must be validated separately, such as SGEMP [23][24][25].

6.0 Code Documentation

UTDEM documentation of design and implementation is contained in special code comments recognized by the code documentation software Doxygen, which converts them to a set of Hyper-Text Markup-Language (HTML) files. This includes Unified-Modeling Language (UML) like graphical design descriptions as well as detailed descriptions of class data and methods. In this way, documentation stays with the source code and therefore has a better chance of remaining up to date as changes are implemented.

This documentation can be built from a code checkout or release distribution. Intended primarily for the code developer, these pages should help navigate and understand the UTDEM implementation.

7.0 Conclusions

The NEVADA-framework implementation of the unstructured FEM solver has demonstrated results which are identical to those of the legacy code VOLMAX with performance degradation of a factor of 2-3, and most of that can be traced to the CG FEM system solve itself. In return, great scalability has been achieved on distributed parallel computing platforms over the limited SMP scalability of VOLMAX, along with improved code design, configuration management, and V&V processes.

8.0 Appendix A: Input Files for Verification Problems

The following are the input files for the verification problems described in the Verification section. They should provide the user with insight into usage and syntax for the UTDEM portion of EMPHASIS/NEVADA. As given, these will produce results very close to those of VOLMAX. To get machine precision agreement, the time steps must be synchronized exactly between the two codes. The input file for UCAVABC_SLOTS in Section 9.5 contains the keyword "CONSTANT TIME STEP" which is used to force the VOLMAX time step on UTDEM.

8.1 UCAVITY Input

```
TITLE
  Unstructured 3D cavity with edge source and observer

UNSTRUCTURED TD ELECTROMAGNETICS
  formulation, second order
  pec bc, sideset 1
  observer, nodeset 16
  source, nodeset 17, gaussian, scale 1. width 2.e-9 peaktime 4.0e-9

  BLOCK 111
    MATERIAL 1
  END

  GRADUAL STARTUP FACTOR 1.0
END

TERMINATION TIME 9.0e-9

aztec
  solver,    cg
  precond,   jacobi
  output,    none
  tol        = 1.e-9
  polynomial order, 1
end

units, si

$
$---------------------------------------------------------------------
$                      P L O T T I N G
$---------------------------------------------------------------------
$
EMIT SCREEN, CYCLE INTERVAL = 1
EMIT PLOT, CYCLE INTERVAL = 2
PLOT VARIABLE
  ELECTRIC_FIELD
END
```

```
$
$-----------------------------------------------------------------------
$                    M A T E R I A L S
$-----------------------------------------------------------------------
$
MATERIAL 1
  model 1
END

MODEL 1 SIMPLE ELECTRICAL
  EPS 1.
  MU 1.
  SIGMA 0.
END

EXIT
```

8.2 UCAVABC Input

```
TITLE
  Unstructured 3D cavity (ABC, not PEC) with edge source and observer

UNSTRUCTURED TD ELECTROMAGNETICS
  formulation, second order
  abc bc, sideset 61
  observer, nodeset 16
  source, nodeset 17, gaussian, scale 1. width 2.e-9 peaktime 4.0e-9

  BLOCK 111
    MATERIAL 1
  END

  GRADUAL STARTUP FACTOR 1.0
END

TERMINATION TIME 9.0e-9

aztec
  solver,    cg
  precond,   jacobi
  output,    none
  tol        = 1.e-9
  polynomial order, 1
end

units, si

$
$-----------------------------------------------------------------------
$                    P L O T T I N G
$-----------------------------------------------------------------------
$
EMIT SCREEN, CYCLE INTERVAL = 1
```

```
EMIT PLOT, CYCLE INTERVAL = 2
PLOT VARIABLE
  ELECTRIC_FIELD
END
$
$-----------------------------------------------------------------
$                       M A T E R I A L S
$-----------------------------------------------------------------
$
MATERIAL 1
  model 1
END

MODEL 1 SIMPLE ELECTRICAL
  EPS 1.
  MU 1.
  SIGMA 0.
END

EXIT
```

8.3 UCAVABC_2MAT_LOSS Input

```
TITLE
  Unstructured 3D cavity (ABC, not PEC) with 2 lossy materials, edge source, and observer

UNSTRUCTURED TD ELECTROMAGNETICS
  formulation, second order
  abc bc, sideset 2
  observer, nodeset 16
  source, nodeset 17, gaussian, scale 1. width 2.e-9 peaktime 4.0e-9

  BLOCK 1
    MATERIAL 1
  END

  BLOCK 22
    MATERIAL 2
  END

  GRADUAL STARTUP FACTOR 1.0
END

TERMINATION TIME 9.0e-9

aztec
  solver,    cg
  precond,   jacobi
  output,    none
  tol        = 1.e-9
  polynomial order, 1
end
```

```
units, si

$
$----------------------------------------------------------------------
$                    P L O T T I N G
$----------------------------------------------------------------------
$
EMIT SCREEN, CYCLE INTERVAL = 1
EMIT PLOT, CYCLE INTERVAL = 2
PLOT VARIABLE
 ELECTRIC_FIELD
END
$
$----------------------------------------------------------------------
$                    M A T E R I A L S
$----------------------------------------------------------------------
$
MATERIAL 1
 model 1
END

MATERIAL 2
 model 2
END

MODEL 1 SIMPLE ELECTRICAL
 EPS 1.2
 MU 1.3
 SIGMA 0.0001
END

MODEL 2 SIMPLE ELECTRICAL
 EPS 1.5
 MU 1.6
 SIGMA 0.0003
END

EXIT
```

8.4 UCAVABC_WIRE Input

```
TITLE
 Unstructured 3D cavity with wire, wire observer, edge source, and observer

UNSTRUCTURED TD ELECTROMAGNETICS
 formulation, second order
 abc bc, sideset 2
 observer, nodeset 28
 source, nodeset 31, gaussian, scale 1. width 2.e-9 peaktime 10.0e-9 direction, x 0. y 0. z -1. length
0.5
 wire, edgeset 115, radius 0.00001, resistance 0.0
 wire observer, nodeset 11
```

```
 BLOCK 1
  MATERIAL 1
 END

 GRADUAL STARTUP FACTOR 1.0
END

EXODUS EDGE SETS 115

TERMINATION TIME 9.0e-9

aztec
 solver,    cg
 precond,   jacobi
 output,    none
 tol        = 1.e-12
 polynomial order,  1
end

units, si

$
$--------------------------------------------------------------------------
$                      P L O T T I N G
$--------------------------------------------------------------------------
$
EMIT SCREEN, CYCLE INTERVAL = 1
EMIT PLOT, CYCLE INTERVAL = 2
PLOT VARIABLE
 ELECTRIC_FIELD
END
$
$--------------------------------------------------------------------------
$                       M A T E R I A L S
$--------------------------------------------------------------------------
$

MATERIAL 1
 model 1
END

MODEL 1 SIMPLE ELECTRICAL
 EPS 1.
 MU 1.
 SIGMA 0.
END

EXIT
```

8.5 UCAVABC_SLOTS Input

```
TITLE
 Unstructured 3D cavity with slots, slot observers, edge source, observer,
```

```
and outer ABC boundary

UNSTRUCTURED TD ELECTROMAGNETICS
  formulation, second order
  abc bc, sideset 4
  pec bc, sideset 2
  observer, nodeset 28
  observer, nodeset 29
  source, nodeset 31, gaussian, scale 1. width 2.e-9 peaktime 10.0e-9
  slot observer, nodeset 19
  slot, edgeset 123, width 0.00001, depth 0.0, int_mat 1, ext_mat 2
  slot observer, nodeset 20
  slot, edgeset 124, width 0.00005, depth 0.0, int_mat 1, ext_mat 2

  CONSTANT TIME STEP 1.01197539e-09
  GRADUAL STARTUP FACTOR 1.0

BLOCK 1
    MATERIAL 1
  END
  BLOCK 22
    MATERIAL 2
  END
END

EXODUS EDGE SETS (123 124 153)
TERMINATION TIME 9.0e-9

aztec
  solver,    cg
  precond,   jacobi
  output,    none
  tol        = 1.e-12
  polynomial order,  1
end

units, si

$
$---------------------------------------------------------------------
$                      P L O T T I N G
$---------------------------------------------------------------------
$
EMIT SCREEN, CYCLE INTERVAL = 1
EMIT PLOT, CYCLE INTERVAL = 2
PLOT VARIABLE
  ELECTRIC_FIELD
END
$
$---------------------------------------------------------------------
$                      M A T E R I A L S
$---------------------------------------------------------------------
$
```

```
MATERIAL 1
  model 1
END

MATERIAL 2
  model 2
END

MODEL 1 SIMPLE ELECTRICAL
  EPS 1.
  MU 1.
  SIGMA 0.
END

MODEL 2 SIMPLE ELECTRICAL
  EPS 1.
  MU 1.
  SIGMA 0.
END

EXIT
```

8.6 UCOAX_BELT Input

```
TITLE
  Unstructured 3D coax with distributed belt source, e-line integral observers,
and ABC boundaries on end caps

UNSTRUCTURED TD ELECTROMAGNETICS
  formulation, second order
$ pec specifications must come first if they will touch abc, ibc, etc.
  pec bc, sideset 8
  pec bc, sideset 9
  abc bc, sideset 11
  abc bc, sideset 12
  observer, edgeset 151, direction, x -1. y 0. z 0.
  observer, edgeset 152, direction, x 0. y 0. z 1.
  source, sideset 14, gaussian, scale 1. width 1.e-11 peaktime 5.0e-11 direction, x 0. y 1. z 0. length
0.0005

  BLOCK 1
    MATERIAL 1
  END

  GRADUAL STARTUP FACTOR 1.0
END

EXODUS EDGE SETS (151 152)
TERMINATION TIME 1.0e-11

aztec
  solver,    cg
  precond,   jacobi
```

```
  output,    none
  tol        = 1.e-12
  polynomial order,  1
end

units, si

EMIT SCREEN, CYCLE INTERVAL = 1
EMIT PLOT, CYCLE INTERVAL = 2
PLOT VARIABLE
  ELECTRIC_FIELD
END

MATERIAL 1
  model 1
END

MODEL 1 SIMPLE ELECTRICAL
  EPS 2.2
  MU 1.
  SIGMA 0.
END

EXIT
```

9.0 Appendix B: Field Solver Options for PIC Simulations

An important issue for PIC simulations is the very high frequency, short wavelength noise ($\omega \sim \pi/\Delta t$, $k \sim \pi/\Delta x$) generated by particle fluctuations, driven for the most part by particles making cell transitions. The most direct way to reduce the fluctuation level is to reduce the cell size and timestep, and use more particles per cell. Clearly, this is often impractical. An alternative approach is to use a field solver that provides frequency-dependent damping: very low (ideally zero) at physical frequencies of interest, and increasing as $f \rightarrow 1/\Delta t$. Emphasis now has two field solver options with damping, based on well-known algorithms for PIC on structured grids: the Godfrey "time-biased" algorithm [26][27], and the Friedman algorithm [28].

9.1 The Godfrey Field Solver

Godfrey generalized the Newmark time integration that is shown in Equation 17 to include time weighting on the [S] term,

$$[T]\frac{E_c^{n+1} - 2E_c^n + E_c^{n-1}}{\Delta t^2} + [B]\frac{E_c^{n+1} - E_c^{n-1}}{2\Delta t} + [S]\left(\alpha_1 E_c^{n+1} + \alpha_2 E_c^n + \alpha_3 E_c^{n-1}\right) + F] = 0 \tag{B1}$$

This results in an equation that corresponds to Equation 18 in the main text,

$$E^{n+1} - 2E^n + E^{n-1} + 4\Delta t\frac{\left([B] + (2\alpha_1 + \alpha_2)\Delta t[S]\right)E^n + \left(-[B] + \left(1 - (2\alpha_1 + \alpha_2)\right)\Delta t[S]\right)E^{n-1} + \Delta tF])}{4[T] + 2\Delta t[B] + 4\alpha_1\Delta t^2[S]} = 0. \tag{B2}$$

It should be noted that this same weighting could also be include in $F]$ to completely time weight the source terms for this second order update, but this would involve a implicit update for all the particle to get the future time, n+1, for the currents. This step is not done at this time. To maintain second order accuracy, $\alpha_1 + \alpha_2 + \alpha_3 = 1$; to be energy conserving (symplectic), $\alpha_1 = \alpha_3$; and to be unconditional stable, $\alpha_2^2 = 4\alpha_1\alpha_3$. This leads to the Newmark condition of $\alpha_1 = {}^1/_4, \alpha_2 = {}^1/_2, and\ \alpha_3 = {}^1/_4$. For the filtering, the symplectic condition ($\alpha_1 = \alpha_3$) is relaxed and Equation B2 can be simplified to

$$E^{n+1} - 2E^n + E^{n-1} + 4\Delta t\frac{\left([B] + 2\sqrt{\alpha_1}\Delta t[S]\right)E^n + \left(-[B] + \left(1 - 2\sqrt{\alpha_1}\right)\Delta t[S]\right)E^{n-1} + \Delta tF])}{4[T] + 2\Delta t[B] + 4\alpha_1\Delta t^2[S]} = 0. \tag{B3}$$

Figure B1 shows the real and imaginary part of the dispersion for various values of α_1. From this figure one can conclude that the practical range of $\alpha_1$varies of ¼ to a value of 1. For a value of $\alpha_1 = 1/2$, this field solve update corresponds to the Friedman filter (Section

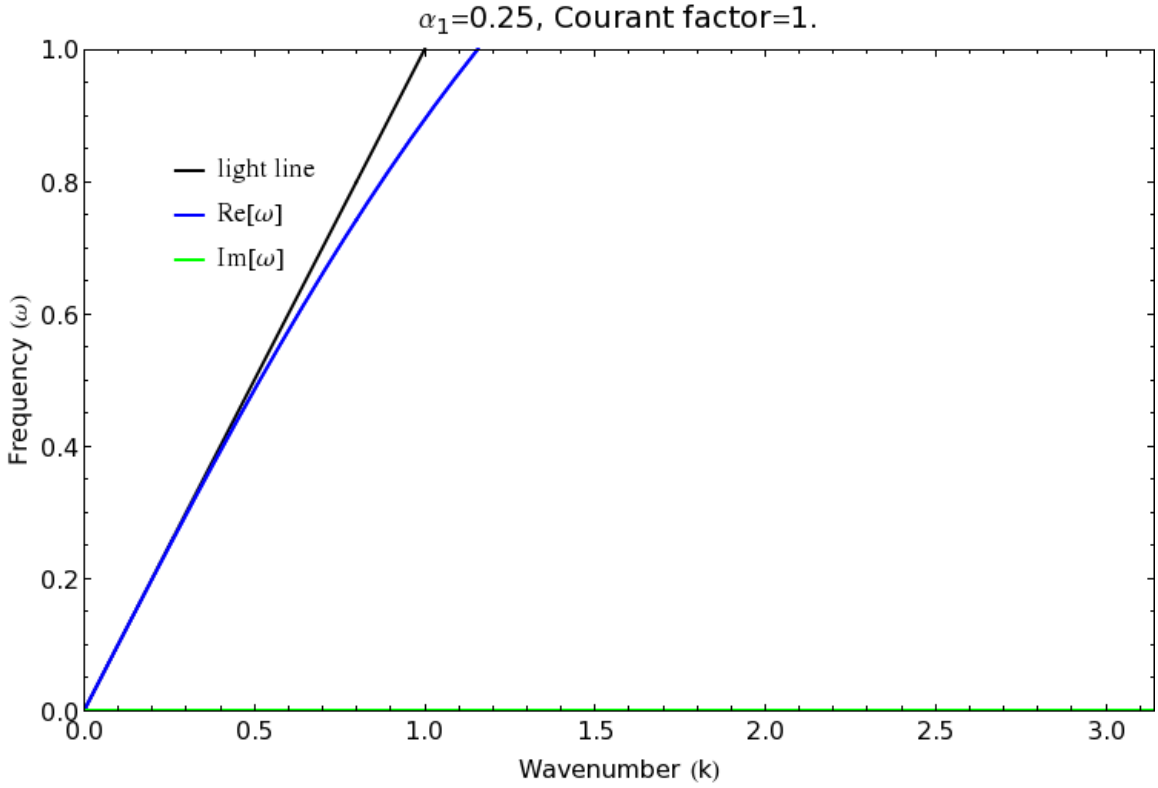

9.2) with at value of θ=2.

Figure 6 . Godfrey numerical dispersion for various values of α_1.

9.2 The Friedman Field Solver

The Friedman solver is based on a digital filtering scheme developed for an implicit particle advance scheme (*i.e.* where the electric field used to advance the particles depends on the final position of the particle). To adapt this to an implicit field solver, we first consider the simple 1-D wave equation in vacuum,

$$\frac{\partial^2 E}{\partial t^2} = c^2 \frac{\partial^2 E}{\partial x^2}. \qquad \text{(B4)}$$

This equation is finite differenced for $E_j^n = E(j\Delta x, n\Delta t)$ using

$$\frac{E^{n+1} - 2E^n + E^{n-1}}{\Delta t^2} = c^2 \nabla_j^2 \frac{1}{2}\left[E^{n+1} + \frac{\theta}{2} E^n + \left(1 - \frac{\theta}{2}\right)\overline{E}^{n-2} \right], \tag{B5}$$

where the *j* subscript on *E* has been dropped for simplicity,

$$\nabla_j^2 F_j = \frac{F_{j+1} - 2F_j + F_{j-1}}{\Delta x^2} \tag{B6}$$

is the spatial differencing operator, $0 \le \theta \le 1$ is an adjustable parameter controlling the magnitude of the damping, and

$$\overline{E}^{n-2} = \left(1 - \frac{\theta}{2}\right) E^{n-1} + \frac{\theta}{2}\overline{E}^{n-3}, \tag{B7}$$

is a recursive lag-average of *E* over all previous timesteps. For a plane wave solution of the form $E_0 exp[i(kx-\omega t)]$, this differencing scheme has the dispersion relation

$$\frac{(1-\alpha)^2 (2 - \theta/\alpha)}{\alpha^2 + 1 - \theta} = -4\nu^2 \sin^2\left(\frac{k\Delta x}{2}\right) = -\Lambda, \tag{B8}$$

where $\alpha = exp[-i\omega\Delta t]$, and $\nu = c\Delta t/\Delta x$ is the Courant number. Eq. (B6) is a cubic equation for $\alpha(k)$, and analysis shows that the scheme is unconditionally stable for all values of ν, and is highly dispersive and strongly damped when $\Lambda >> 1$. For long wavelengths, as $\Lambda \to 0$, one of the roots, $\omega(k) = \omega_r + i\gamma$, is a weakly damped physical solution,

$$\omega_r / \omega_0 = 1 - \omega_0^2 \Delta t^2 [1/(4 - 2\theta) - 1/24] + \ldots \tag{B9}$$

$$\gamma / \omega_0 = -\theta / [2(2-\theta)^2] \omega_0^3 \Delta t^3 + \ldots \tag{B10}$$

where $\omega_0 = ck$. is the exact frequency. Eq. (B8) shows that $\gamma \sim k^4$, meaning that damping of long wavelength modes drops off very rapidly.

To apply this algorithm to Emphasis, we replace the Newmark-Beta term in Eq. (17) with a form corresponding to the RHS of Eq. (B3),

$$[S]\frac{1}{2}\left[E^{n+1} + \frac{\theta}{2} E^n + \left(1 - \frac{\theta}{2}\right)\overline{E}^{n-2} \right]. \tag{B11}$$

This changes Eq. (18) into the form

$$E^{n+1} - 2E^n + E^{n-1} + 4\Delta t \frac{\left([B] + \left(1 + {}^{\theta}/_{4}\right)\Delta t[S]\right)E^n - E^{n-1}\left([B] + {}^{\Delta t[S]}/_{2}\right) + \Delta t([S]({}^{1}/_{2} - {}^{\theta}/_{4})\bar{E}^{n-2} + \Delta t F])}{4[T] + 2\Delta t[B] + 2\Delta t^2[S]} = 0. \tag{B12}$$

The algorithm requires the extra fields $\overline{E}$, which are updated after the matrix solve, just before E^n is advanced to the new time level.

10.0 Appendix C: Port Source Implementation

The port source contribution is based on an adaptation of a waveguide boundary condition due to Jin [29]. The total field in a waveguide is expressed as a superposition of incident and reflected TE_{10} waves and manipulated into a form mimicking the boundary condition of the third kind,

$$\frac{1}{\mu_r}\hat{n} \times (\nabla \times \bar{E}) + jk\,\hat{n} \times (\hat{n} \times \bar{E}) = \bar{U}$$

The $\bar{U}$ generated by this exercise takes the form

$$\bar{U} = \frac{-2jk}{\mu_r}\bar{E}^{inc}$$

In accordance with the variational formulation functional term (e.g. Jin Eq. 8.82)

$$\int_{S_{port}} \bar{E} \cdot \bar{U}\, ds$$

and converting to the time domain, this leads to the following term being added to the rhs of equation (15):

$$\int_{S_{port}} \frac{-2\sqrt{\mu_r \epsilon_r}}{c\mu_r} \bar{W}_i \cdot \frac{\partial \bar{E}^{inc}}{\partial t}\, ds = \int_{S_{port}} \frac{-2}{c}\sqrt{\frac{\epsilon_r}{\mu_r}} \bar{W}_i \cdot \frac{\partial \bar{E}^{inc}}{\partial t}\, ds$$

11.0 References

[1] C. D. Turner, Preliminary Evaluation of Software Frameworks for EMPHASIS, memo to M. L. Kiefer, Dec. 1999.

[2] J. F. Lee and Z. Sacks, Whitney Elements Time Domain (WETD) Methods, IEEE Trans. Magnetics, Vol. 21, No. 3, May 1995.

[3] O. C. Zienkiewicz and R. L. Taylor, The Finite Element Method, Butterworth-Heinemann, 5th edition, 2000, Ch. 18.

[4] H-P. Tsai, Y. Wang, T. Itoh, An Unconditionally Stable Extended (USE) Finite-Element Time-Domain Solution of Active Nonlinear Microwave Circuits Using Perfectly Matched Layers, IEEE Trans. Microwave Theory and Techniques, Vol. 50, No. 10, October 2002.

[5] W. A. Artuzi, Improving the Newmark Time Integration Scheme in Finite Element Time Domain Methods, IEEE Microwave and Wireless Components Letters, Vol. 15, No. 12, December 2005.

[6] M. Wong, O. Picon, and V. F. Hanna, A Finite Element Method Based on Whitney Forms to Solve Maxwell Equations in the Time Domain, IEEE Trans. Magnetics, Vol. 31, No. 3, May 1995.

[7] J. Jin, The Finite Element Method in Electromagnetics, Wiley, 1993, p. 251.

[8] J. P. Webb, Hierarchal Vector Basis Functions of Arbitrary Order for Triangular and Tetrahedral Finite Elements, IEEE Trans. Ant. Prop., Vol. 47, No. 8, August 1999.

[9] R. D. Graglia and I. L. Gheorma, Higher Order Interpolatory Vector Bases on Pyramidal Elements, IEEE Trans. Ant. Prop., Vol. 47, No. 5, May 1999.

[10] F.-X. Zgainski, J.-L. Coulomb, and Y. Marechal, A New Family of Finite Elements: The Pyramidal Elements, IEEE Trans. Magnetics, Vol. 32, No. 3, May 1996.

[11] Jin, p. 253.

[12] D. E. Merewether, Finite Difference Solution of Maxwell's Equation for EMP Applications, Defense Nuclear Agency Final Report, Contract No. DNA 001-78-C-0231, April 1980.

[13] Jin, p. 91-92.

[14] J. Jin and D. J. Riley, Finite Element Analysis of Antennas and Arrays, Wiley, 2009, p. 201-208.

[15] L. K. Warne and K. C. Chen, Equivalent Antenna Radius for Narrow Slot Apertures Having Depth, IEEE Trans. Ant. Prop., Vol. 37, No. 7, 1989.

[16] Jin, p. 325.

[17] D. J. Riley and C. D. Turner, The VOLMAX Transient Electromagnetic Modeling System, Including Sub-Cell Slots and Wires on Random Non-Orthogonal Cells, SAND97-2906C, Applied Computational Electromagnetics Society (ACES) Symposium, Monterey, CA, March 1998.

[18] D. J. Riley, HEART 2000 Short Course: Enhanced Use of Simulation and Modeling for Radiation Hardening, SAND99-3037, 2000 HEART conference, Alexandria, VA, Nov. 1999.

[19] R. C. Pate, D. J. Riley, P. E. Patterson, E. S. Kunhardt, T. Hussey, S. Macgregor, Modeling High-Speed Discharge Switching for Wideband and Ultra-Wideband Applications Using a Transient, Full-Wave Electromagnetic Solver with an Integrated Gas-Discharge Physics Model, SAND2000-0405A, 2000 IEEE Int. Symp. on Ant. Prop. / URSE Nat. Radio Sci. Meeting, Salt Lake City, UT, July 2000.

[20] D. J. Riley, Transient Finite-Elements for Computational Electromagnetics: Hybridization with Finite Differences, Modeling Thin Wires and Thin Slots, and Parallel Processing, Applied Computational Electromagnetics Society (ACES) Symposium, SAND2001-0566C, Monterey, CA, March 2001.

[21] D. J. Riley, VOLMAX Verification and Validation Suite I, Northrop Grumman Mission Systems Report to Sandia National Laboratories under contract number 30403, Albuquerque, NM, Dec. 2002.

[22] C. D. Turner, G. J. Scrivner, CABANA Serial/Development Version Description, Verification, and Validation, SAND2001-3567, November 2001.

[23] Laura P. Swiler, Wesley C. Fan, C. David Turner, William L. Oberkamph, Jon C. Helton, “Uncertainty Analysis for Electrical Cables in Radiation Environments”, ASC Tri-Lab Conference, May 10, 2007.

[24] Laura P. Swiler, Wesley C. Fan, C. David Turner, William J. Bohnhoff, “2008 ASC Milestone 2842: Uncertainty Analysis for an RB Electrical Cable in Radiation Environments”, ASC L2 V&V Milestone Final Review, 27 August 2008.

[25] B. C. Franke, W. C. Fan, T. D. Pointon, D. B. Seidel, M. Caldwell, M. F. Pasik, C. D. Turner, “FY11 ASC L2 Milestone 3967 Cavity SGEMP V&V Final Documentation Set”, SAND2010-8722P, December 2010.

[26] B. B. Godfrey. Time-biased field solver for electromagnetic PIC codes, in: Proceedings of the Ninth Conference on Numerical Simulation of Plasmas, 1980.

[27] A. D. Greenwood, K. L. Cartwright, J. W. Luginsland, E. A. Baca, On the elimination of numerical Cerenkov radiation in PIC simulations, J. Comput. Phys. **201**, 665-684 (2004).

[28] A. Friedman, A Second-Order Implicit Particle Mover with Adjustable Damping, J. Comput. Phys. **90**, 292-312 (1990).

[29] Jin, pp. 263-265

Distribution

Email—Internal

Name	Org.	Sandia Email Address
K. L. Cartwright	01351	klcartw@sandia.gov
J. D. Kotulski	01351	jdkotul@sandia.gov
T. D. Pointon	01351	tdpoint@sandia.gov
C. D. Turner	01351	cdturne@sandia.gov
Technical Library	01177	libref@sandia.gov

Sandia National Laboratories

Sandia National Laboratories is a multimission laboratory managed and operated by National Technology & Engineering Solutions of Sandia LLC, a wholly owned subsidiary of Honeywell International Inc. for the U.S. Department of Energy's National Nuclear Security Administration under contract DE-NA0003525.